INTERNATIONAL APPLICATION PUBLISHED UNDER THE PATENT COOPERATION TREATY (PCT)

(72) Inventors; and
(75) Inventors/Applicants *(for US only)*: PERELMAN, Lev, T. [US/US]; 94 Griggs Road #21, Brookline, MA 02146 (US). BACKMAN, Vadim [RU/US]; Apartment 9E1, 550 Memorial Drive, Cambridge, MA 02139 (US). FELD, Michael, S. [US/US]; 56 Hinckley Road, Newton, MA 02168 (US). ZONIOS, George [GR/US]; 305 Memorial Drive #205B, Cambridge, MA 02139 (US). ITZKAN, Irving [US/US]; 330 Beacon Street, Boston, MA 02116 (US).

MANOHARAN, Ramasamy [IN/US]; 25 Homer Avenue #12, Cambridge, MA 02138 (US).

(74) Agents: HOOVER, Thomas, O. et al.; Hamilton, Brook, Smith & Reynolds, P.C., Two Militia Drive, Lexington, MA 02421 (US).

(54) Title: METHOD FOR MEASURING TISSUE MORPHOLOGY

(57) Abstract

An apparatus for measuring one or more physical characteristics of material by means of optical radiation scattered by a tissue layer to determine, for example, the size of nuclei in a tissue layer. The apparatus includes fiber optic devices (10, 20, 30) to deliver and collect light from a tissue region of interest to determine, for example, whether the tissue is normal or precancerous.

METHOD FOR MEASURING TISSUE MORPHOLOGY

GOVERNMENT SUPPORT

RELATED APPLICATIONS

This is a continuation-in-part of U.S. Serial No. 08/948,734 filed on October 10, 1997, the entire contents

10 of which is incorporated herein by reference.

BACKGROUND OF THE INVENTION

Methods for diagnosis of cancer at an early stage are essential for cancer prevention and therapy. Many types of cancers grow from epithelial tissues, which cover inner and

-2-

outer surfaces of the human body. Many of these, for
example cancer in gastrointestinal tract, progress through
the stage of dysplasia. Dysplasia can be defined as
neoplastic tissue which is not malignant yet, but is
5   considered to be a precursor of malignancy. If diagnosed
at this stage, most tumors are curable. In the case of
gastrointestinal tumors, current methods of diagnosis are
based on endoscopy. However, dysplastic tissue is
frequently not endoscopically apparent. Thus, detection of
10 dysplasia in the gastrointestinal tract and other sites
often relies on sporadic sampling for this "invisible"
malignant precursor. However, sporadic biopsies have a
high probability of missing dysplastic changes. In some
cases the biopsy procedure is impossible.

15   Efforts toward a substitution for standard biopsies
have been made in order to provide accurate diagnosis of
cancerous tissue in different organs *in vivo* and in real
time. For this purpose, optical techniques that are non-
invasive do not require tissue removal and can be performed
20 in-vivo. Such methods provide information at the
microscopic level and can thus provide for the search for
very small sites which are likely to be missed by standard
biopsies. While most human organs can be diagnosed by
means of optical techniques, they are particularly
25 applicable to the tissues in human body lumene, since they
are easily accessible by optical probes, which can be

-3-

inserted into one of the channels of a conventional
endoscopic tube.

SUMMARY OF THE INVENTION

The present invention relates to the use of light to
5   determine physical characteristics of a structured layer of
material, and in particular certain qualitative information
regarding the morphology of tissue structures using
scattered light. Both backscattered and transillumination
methods can be used, depending upon the thickness of the
10   material and the size and distribution of the structure
being measured. Examples of properties of materials that
can be measured include surface roughness, parasity,
cytometer measurements, or any material in which changes in
the refractive index of a material correspond to changes in
15   structures. This type of scattering spectroscopy can be
differentiated from absorption spectroscopy which is unable
to quantitatively measure particle morphology.

Despite extensive investigations, no reliable optical
technique to diagnose dysplasia in-vivo is known. One of
20   the difficulties resides in the fact that dysplastic
changes are limited to the uppermost epithelial layer,
which can be as thin as $20 \mu m$, a one cell layer that is
nearly transparent to optical radiation.

Tissue in the gastrointestinal tract, for example
25   (other hollow organs share the same features also), is
covered by a layer of cells called epithelium (from $20 \mu m$

-4-

to 300µm thick depending on the part of the tract)
supported by relatively acellular and highly vascular loose
connective tissue, lamina propria, which can be up to
500µm in thickness and contains a network of collagen and
5   elastic fibers, and variety of white blood cell types.
Beneath the lamina propria there is a muscular layer,
muscularis mucosae, (up to 400µm thick) and another layer
of moderately dense connective tissue called submucosa
(400-600µm thick) containing many small blood vessels and
10 abundant collagen and elastic fibers. The overall
thickness of those layers is about 1mm. Since a
characteristic penetration depth of optical radiation into
biological tissue does not usually exceed 1mm, for a
preferred embodiment it is sufficient to limit measurements
15 of tissue by those layers.
        Adenocarcinoma of the esophagus arises in metaplastic
columnar epithelial cells in the esophagus, termed
"Barrett's esophagus", which is a complication of long-
standing gastrointestinal reflux. In this condition, the
20 distal squamous epithelium is replaced by columnar
epithelium consisting of a one cell layer which resembles
that found in the intestines. Barrett's esophagus is
frequently associated with dysplasia which later can
progress to cancer. Trials of endoscopic surveillance of
25 patients with Barrett's esophagus have not resulted in a
reduction of esophageal cancer mortality. The most likely
explanation is that dysplasia occurring in the esophagus

-5-

cannot be seen with standard endoscopic imaging and
sporadic biopsy sampling is necessary. This procedure can
sample only about 0.3% of the tissue at risk. Thus, there
is tremendous potential for sampling error.

5   The application of optical techniques to diagnose
dysplasia in Barrett's esophagus is limited by the fact
that the primary alterations in the tissue occur in the
epithelium which is one cell thick (~20-30μm) while
fluorescence or reflectance spectra are mostly formed in
10   deeper tissue layers. One of the most prominent features
of a dysplastic epithelium is the presence of enlarged,
hyperchromatic, and crowded nuclei. In fact, these changes
in nuclei size and spatial distribution are the main
markers used by a pathologist to diagnose a tissue specimen
15   as being dysplastic. No significant changes in other
tissue layers is observed. Unfortunately, epithelium does
not contain strong absorbers or fluorophores, and the
thickness of the epithelium is relatively small and thus
negligible. These make epithelium diagnosis in Barrett's
20   esophagus to be a difficult problem.

         Diffuse reflectance spectroscopy can provide
quantitative biochemical and morphological information for
the analysis of biological tissue epithelium and the
detection of precancerous lesions. Diffuse reflectance
25   spectra were collected from adenomatous colon polyps
(cancer precursors) and normal colonic mucosa of patients
undergoing colonoscopy. The data were analyzed using an

-6-

analytical light diffusion system, which was measured on a
physical tissue model composed of polystyrene beads and
hemoglobin. Four parameters were obtained: hemoglobin
concentration, hemoglobin oxygen saturation, effective
5   scatterer density, and effective scatterer size. Normal
and adenomatous tissue sites exhibited differences in
hemoglobin concentration and effective scatterer size.
Thus, diffuse reflectance can be used to obtain tissue
biochemical and morphological information *in vivo*.

10   A preferred embodiment of the present invention
relates to a system of measuring a fine structure component
in backscattered light from mucosal tissue which is
periodic in wavelength. This structure is ordinarily
masked by a diffusive background, which must be removed to
15   render it observable. The origin of this component is due
to light which is Mie-scattered by surface epithelial cell
nuclei. By analyzing the amplitude and frequency of the
periodic structure, the density and size distribution of
these nuclei can be extracted. These quantities are
20   important indicators of neoplastic precancerous changes in
biological tissue, and the technique can thus provide a
useful tool for observing such changes in patients
undergoing endoscopy.

        The light that is incident on the thin layer at the
25   tissue surface is not completely randomized. In this thin
region the details of the elastic scattering process can be
preserved. Mucosal tissues, which line the hollow organs

-7-

of the body, generally consist of a thin surface layer of
epithelial cells supported by underlying, relatively
acellular connective tissue. In healthy tissues the
epithelium often consists of a single, well-organized layer
5   of cells with an endface diameter of about 10-20 μm and a
height of about 25 μm. In cancerous and pre-cancerous
(dysplastic) epithelium cells proliferate, the cellular
layer often thickens and becomes more tightly packed, and
the cell nuclei enlarge and appear darker (hyperchromatic)
10 when stained. This may indicate increased nucleic acid
density, hence increased refractive index.

A preferred embodiment of the invention utilizes a
broadband light source to illuminate the region of interest
in the tissue with optical radiation in the range between
15 350 and 700 nm. A fiber optic probe can be used to deliver
and/or collect radiation from the tissue. The system can
be used during endoscopy of a patient to optically survey a
body lumen within the patient and thereby eliminate the
need for removal·of tissue for biopsy, or alternatively,
20 can be used to aid in locating tissue suitable for biopsy.

Backscattered light is preferably collected over a
small collection angle of between 2° and 12°, preferably in
the range between 3° and 8°. When using an optical fiber
system to collect the scattered light fibers having a
25 numerical aperture between 0.05 and 0.22, and preferably
between 0.07 and 0.1 can be used. Collection angles within

-8-

this range reduce the level of background light without
loss of the periodic component in the returning light.

BRIEF DESCRIPTION OF THE DRAWINGS

Figure 1 is a schematic diagram of a fiber optic probe
5   in accordance with the invention.

Figure 2 is an enlarged view of the distal end of an
endoscope in accordance with the invention.

Figures 3A, 3B and 3C illustrate reflectance spectra
from cell monolayers for normal colon cells ($\bar{R} = 0.46$);
10   T84 cells ($\bar{R} = 0.38$); (c) BaSO$_4$ diffusing plate ($\bar{R} = 1.0$)

Figure 4 illustrates nuclear size distributions from
data of Figures 3A and 3B, respectively for normal colon
cells; and T84 cells respectively. In each case, the solid
line is the distribution extracted from the data, and the
15   dashed line is the distribution measured using light
microscopy.

Figures 5A, 5B and 5C are reflectance spectra from
Barretts' esophagus for diffuse reflectance from a normal
site (solid line), a dysplastic site (dashed line), and the
20   model fit (thick solid line); for corresponding fine
structures; and of resulting nuclear size distributions,
respectively.

Figure 6 graphically illustrates a comparison of
samples analyzed by standard pathology and the optical
25   methods in accordance with the invention.

-9-

Figure 7 is a system used for *in vitro* tissue analysis in accordance with the invention.

Figure 8 is a process flow diagram illustrating a method of performing an optical diagnosis of tissue in
5   accordance with the invention.

Figure 9 is the molar extinction coefficient spectra (per heme group) of the oxygenated (thin line0 and deoxygenated (thick line) hemoglobin (21). Note the characteristic peaks at 415, 542, and 577 nm
10   (oxyhemoglobin-HbO$_2$) and at 430 and 555 nm (deoxyhemoglobin-Hb).

Figure 10 is the reduced scattering cross section spectra σ' (λ), calculated using Mie theory. Results are shown for four different diameters, d$_s$, (0.2, 0.6, 1.0, and
15   2.0 μm). The slope of the spectra is inversely related to the diameter. A refractive index of 1.4 was assumed for the scattering particles, and 1.36 for the surrounding medium.

Figure 11 shows the Diffuse reflectance spectra
20   measured on physical tissue models (thick line) corresponding to four different Hb concentrations: (a) 0.0 mg/dL, (b) 50 mg/dL, (c) 125 mg/dL, (d) 250 mg/dL. The analytical model predictions using the same optical parameters employed in the preparation of the physical
25   tissue models are also shown (thin line), with agreement between the analytical and the tissue model being very good.

-10-

Figure 12 shows the typical normal and adenomatous polyp spectra (thick line), and best fits to the data using the model (thin line). Mie theory was used to approximate the reduced scattering coefficient used for the model fits
5   (see Figure 13).

Figure 13 shows the scattering spectra obtained from the data shown in Figure 12 (thin line), and best fits using Mie theory (thick line). The Mie theory fits assign an effective scatterer size d_s to the reduced scattering
10   spectra. The polyp is characterized by a larger effective scatterer size (d_s = 1.5 μm) as compared to normal mucosa (d_s = 0.35 μm).

Figure 14A-14D show parameters obtained from data analysis: (A) total Hb concentration. C_{Hb}, (B) Hb oxygen
15   saturation, α (C) effective scatterer density, p_s, and (D) effective scatterer size, d_s. The largest difference between normal mucosa (squares) and adenomatous polyps (stars) is observed in the total Hb concentration.

Figure 15 is a binary plot of the total Hb
20   concentration C_{Hb} vs. the effective scatterer size d_s,. The normal data tend to form a well defined cluster, while the adenomatous polyp data are marked by wider variation.

The foregoing and other objects, features and advantages of the invention will be apparent from the
25   following more particular description of preferred embodiments thereof, as illustrated in the accompanying drawings in which like reference characters refer to the

-11-

same parts throughout the different views. The drawings
are not necessarily to scale, emphasis instead being placed
upon illustrating the principles of the invention.

DETAILED DESCRIPTION OF THE INVENTION

5   A preferred embodiment of the invention involves the
use of a fiber optic system to deliver and collect light
from a region of interest to measure one or more physical
characteristics of a surface layer. Such a system is
illustrated in Figure 1. This system can include a light

10   source 50 such as a broadband source, a fiber optic device
10 for delivery and/or collection of light from the tissue,
a detector system 80 that detects the scattered light from
the tissue, a computer 120 having a memory 122 that
analyzes and stores the detected spectra, and a display 124

15   that displays the results of the measurement. A lens 60
can be used to couple light from the source 50 into the
excitation fiber 30 of the probe 10. A filter 110 and lens
system 90,100 can be used to efficiently couple collected
light to a spectrograph 70. A controller 140 connected to

20   the data processing system 120 can be connected to a clock
and a pulser 150 that controls the light source 50.
         The distal end 15 of the probe 10 is illustrated in
Figure 2 where the central excitation fiber 30 is
surrounded by six peripheral collection fiber 20. The

25   distal end of the device can be enclosed in an optical
shield 25 such as that described in U.S. Patent No.

-12-

5,199,431, the entire contents of which is incorporated
herein by reference. Other endoscopic devices can be used
such as an optical needle as described in the above
referenced patent or as described in U.S. Patent No.

5 5,280,788, the entire contents of which is also
incorporated herein by reference.

The collection fibers 20 preferably have a numerical
aperture in the range of 0.05 to 0.22 in order to provide a
desired collection angle from the material being measured.

10 This aids in reducing background that is removed from
scattering spectrum without loss of the periodic component.

The collection fibers can also be replaced or
supplemented by a distally mounted imaging sensor 35 such
as a charged coupled device or CMOS imager. The sensor has

15 a pixellated structure that is sensitive to the different
colors contained in the scattering spectrum being recorded.
Further details regarding the use of a distally mounted
sensor can be found in U.S. Serial No. 08/745,509 filed on
November 12, 1996, the entire contents of which is

20 incorporated herein by reference.

The backscattered light collected with this system can
be analyzed to determine certain physical characteristics
of epithelial tissue. The relationship between the
collected light and the physical characteristics to be

25 determined using this light can be described as follows.

Epithelial nuclei can be represented as spheroidal Mie
scatterers with a refractive index higher than that of the

-13-

surrounding cytoplasm. Normal nuclei have a characteristic

diameter $l=4\text{-}7\mu m$. In contrast, dysplastic nuclei can be

as large as 20 μm in size, occupying almost the entire

cell volume. Thus, in the visible range, the wavelength

5    $\lambda << l$, and the component of light scattered by the nuclei

will exhibit a periodicity with wavelength, the details of

which are determined by the nuclear size distribution. The

Van de Hulst approximation can be used to describe the

optical scattering cross section of the nuclei:

10   $$\sigma_s(\lambda,l) = \frac{1}{2}\pi l^2 \left\langle 1 - \frac{\sin(2\delta/\lambda)}{\delta/\lambda} + \left\langle \frac{\sin(\delta/\lambda)}{\delta/\lambda} \right\rangle^2 \right\rangle,\tag{1}$$

where $\delta = \pi l n_c (n-1)$, with n_c the refractive index of

cytoplasm and n the refractive index of the nuclei relative

to that of cytoplasm.

When a beam of light is incident on an epithelial

15   layer of tissue, a portion of this light is backscattered

from the epithelial nuclei, while the remainder is

transmitted to deeper tissue layers, where it undergoes

multiple scattering and becomes randomized. All of the

diffusive light which is not absorbed in the tissue

20   eventually returns to the surface, passing once more

through the epithelium, where it is again subject to

scattering from the cell nuclei. Thus, the emerging light

consists of a large diffusive background plus the component

of forward scattered and backscattered light from the

25   nuclei in the epithelial layer. For a thin slab of

-14-

epithelial tissue containing nuclei with size distribution
N(l) (number of nuclei per unit area (mm²) and per unit
interval of nuclear diameter (μm)), the approximate
solution of the transport equation for the reflectance
5   R(λ) collected by an optical probe with acceptance solid
angle Ω_c is given by the following expression:

$$\frac{R(\lambda)}{R(\lambda)} = e^{-r(\lambda)} + 1 - \frac{e - r(\lambda)}{I_d(\lambda,s)_{\Omega_c}} \langle I_i(\lambda,-s')p(\lambda,s,-s') \rangle_{\Omega_i} + \langle I_d(\lambda,s')_2 \pi \rangle_{\Omega_c} \qquad (2)$$

where I_i ((λ,s)) is the intensity of the incident light
delivered in solid angle Ω_i, $I_d(\lambda,s)$ is the intensity of the
10 light emerging from the underlying tissue, and

$\langle I(s) \rangle \Omega = \int_\Omega I(s)ds$ for any function I(s) and solid angel Ω,

with s a unit vector pointing outward from the tissue
surface in an arbitrary direction. The quantity

$\bar{R}(\lambda) = \langle I_d(\lambda,s) \rangle_{\Omega_c} / \langle I_i(\lambda,s) \rangle_{\Omega_c}$ is the reflectance of the

15 diffusive background. The optical distance

$\tau(\lambda) = \int_0^\infty \sigma_s(\lambda,l)N(l)dl$ and scattering phase function

$p(\lambda,s,s') = \frac{1}{\tau}\int_0^\infty p(\lambda,l,s,s')\sigma_s(\lambda,l)N(l)dl$ both depend on N(l); for a

sphere, $p(\lambda,l,s,s')$ is determined by Mie theory. The first
term in Eq. (2) describes the attenuation of the diffusive

-15-

background, and the terms in brackets describe
backscattering of the incident light and forward scattering
of diffusive background by the epithelial cell nuclei,
respectively.

5   For small Ω_c the forward scattering term in Eq. (2)

can be expanded in $\tau(\lambda)$. Thus, $\left\langle\left\langle I_d(\lambda,s')\right\rangle_{2\pi}\right\rangle_{\Omega_c} / \left\langle I_d(\lambda,s)\right\rangle_{\Omega_c} \cong f_o + f_1\tau/\tau_o$,

with $\tau_o = \pi/2\int_o^\infty 1^2 N(1)dl$. It is found numerically that $f_1 << f_0$ and

that f_0 and f_1 are approximately independent of wavelength

in the range of interest $(\lambda_{min} = 360$ to $\lambda_{max} = 685nm)$. Similarly,

10   for the backscattering term

$$\left\langle\left\langle I_i(\lambda,-s')p(\lambda,s-s')\right\rangle_{\Omega_i}\right\rangle_{\Omega_c} / \left\langle I_d(\lambda,s)\right\rangle_{\Omega_c} \cong b_o - b_1\tau/\tau_o.$$ Note that in the

forward scattering contribution the first order term

oscillates in phase with $\tau(\lambda)$ as required by the optical

theorem, whereas for the backscattering contribution it is

15   out of phase. Thus, Eq. (2) reduces to

$$\frac{R(\lambda)}{\overline{R}(\lambda)} = e^{-\tau(\lambda)} + (1-e^{-\tau(\lambda)})\left\langle f_1 + b_0 + (f_1 - b_1)\frac{\tau(\lambda)}{\tau_0(\lambda)}\right\rangle,   \qquad (3)$$

which shows that the epithelial nuclei introduce a periodic
fine structure component into the reflectance with a
wavelength dependence similar to that of the corresponding

20   scattering cross section. Its periodicity is approximately
proportional to nuclear diameter, and its amplitude is a

-16-

function of the size and number of nuclei in the epithelial
layer. These quantities can be determined by analyzing the
reflectance, $R(\lambda)$.

    As example of the effects described by Eq. (2),
5   elastic light scattering from normal T84 tumor human
colonic cell monolayers (10 and 15 sites respectively) was
measured and analyzed. The cells, approximately $15\,\mu m$
long, were affixed to glass slides in buffer solution and
placed on top of a $BaSO_4$ diffusing (and highly reflective)
10 plate. The $BaSO_4$ plate was used to approximate the diffuse
reflectance from underlying tissue. The diameters of the
normal cell nuclei generally ranged from 5 to 7 μm and
those of the tumor cells from 7 to $16\,\mu m$.

    An optical fiber probe was used to deliver white light
15 from a xenon arc flashlamp to the samples and collect the
return reflectance signal, as shown in Figure 1. The probe
tip, 1 mm in diameter, consisted of a central delivery
fiber surrounded by six collection fibers, all of which
were covered with a 1 mm thick quartz optical shield. The
20 fibers were 200 μm core fused silica, NA=0.22

$\left(\Omega_i = \Omega_c = \pi NA^2\right).$ To eliminate specular reflection, the probe

was beveled at 17^0 to the normal. At the proximal end the
collection fibers were arranged in a line and imaged onto
the input slit of a spectrograph. A diode array detector
25 recorded the reflectance spectra from 360 to 685 nm.

-17-

Figures 3A and 3B show the normalized reflectance $R(\lambda)/\bar{R}(\lambda)$ from normal and T84 tumor cell samples, respectively. Distinct spectral features are apparent. For comparison, the reflectance spectrum from the $BaSO_4$

5   plate by itself is also shown in Figure 3C. This spectrum lacks structure and shows no prominent features.

To obtain information about the nuclear size distribution from the reflectance data, Eq. (3) needs to be inverted. The nuclear size distribution, N(1), can then be

10   obtained from the Fourier transform of the periodic component of the optical distance $\tau - \tau_o \cong (1 - R(\lambda))/q$. The parameter q = 1 - b_0 - f_0 +2(b_1 - f_1) is associated with forward and backward scattering, and depends on the probe geometry and the angular distribution of the incident and

15   reflected light. In this particular example q=0.15. By introducing the effective wavenumber k=2Πn_c(n-1)/$\lambda - k_0$, and

$k_o = 2\pi n_c(n-1)/\lambda_{max}, K = 2\pi n_c(n-1)\langle\lambda_{min}^{-1} - \lambda_{max}^{-1}\rangle$ and we obtain,

$$N(1) \cong \frac{2}{q l \pi^2} \int_o^K \left\langle \frac{R(k)}{\bar{R}(k)} - 1 \right\rangle e^{ikl}(k + k_o)dk. \tag{4}$$

Equation (4) was used to analyze the data. In order to

20   remove spurious oscillations, N(1) was further processed by convolving it with a Gaussian filtering function. The solid curves in Figure 4 show the resulting

-18-

nuclear size distributions of the normal and T84 cell
monolayer samples extracted from the spectra of Figures 3A
and 3B. A nucleus-to-cytoplasm relative refractive index
of n=1.06 and cytoplasm refractive index of n_c=1.36 were

5   used. The dashed curves show the corresponding size
distributions, measured morphometrically via light
microscopy. The size distributions can be approximated by
Gaussian distributions. The parameters for those are
presented in Table 1. The extracted and measured

10   distributions are in good agreement for both normal and T84
cell samples.

Table 1

	Normal Cells		Tumor T84 Cells	
	Mean Diameter (μm)	Standard Deviation (μm)	Mean Diameter (μm)	Standard Deviation (μm)
Microscopy	~6	~0.5	10.2	2.0
Spectroscopy	6.2	0.45	10.1	2.2

15

The periodic fine structure in diffuse reflectance of
esophagus and colon mucosa of human subjects can be
measured during gastroenterological endoscopy procedures.
In the case of Barretts' esophagus, in which the epithelium

20   consists of a thin monolayer of columnar cells similar to
those used in the cell culture experiments, data were
collected as in the cell culture studies. The optical
fiber probe is inserted into the biopsy channel of the
endoscope and brought into contact with the tissue surface.

-19-

The methods described herein can also be used to measure structural properties of other GI tissue, tissues in the oral cavity, the cervix, the bladder, and skin.

The fine structure component, which is the scattering
5   signature of the cell nuclei, is typically less then 5% of the total signal and is ordinarily masked by the background of diffusely scattered light from underlying tissue, which itself exhibits spectral features due to absorption and scattering, as shown in Figure 5A. Its spectral features
10 are dominated by the characteristic absorption bands of hemoglobin and collagen scattering. In order to observe the fine structure, this background must be removed. The absorption length, μ_a^{-1}, ranges from 0.5 to 250 mm as the wavelength is varied, and the effective scattering length
15 $(\mu_s')^{-1}$ ranges from 0.1 to 1 mm. Thus, both scattering and absorption have to be taken into account in subtracting or removing the background signal.

To represent the background light incident on the tissue is assumed to be exponentially attenuated, and that
20 at any given depth, z, an amount of light proportional to the reduced scattering coefficient μ_a is scattered back towards the surface and further exponentially attenuated. Since light attenuation depends on both scattering and absorption, the attenuation coefficient is assumed to be
25 the sum of absorption coefficient μ_a and effective scattering coefficient $\mu_s^{(e)} = \beta \mu_s'$. The parameter β was

-20-

determined by comparison with Monte Carlo simulations and
more accurate models of light transport, and was found to
be $\beta \approx 0.07$. Since light only penetrates ~1 mm into the
tissue, most of the diffusely scattered return light is
5   confined to the mucosal layer.

The tissue is thereby represented as a two layer
medium and neglected diffusely reflected light from the
lower layer. The following approximate expression for the
diffusive light from underlying tissue impinging on the
10 epithelial cell layer is then obtained:

$$I_d(\lambda,s) = F(s)\langle I_i(\lambda,s)\rangle_{\Omega_i} \frac{1-\exp[-(\mu_s^{(e)}+c\mu_a)L]}{1+c(\mu_a/\mu_s^{(e)})} \qquad (5)$$

with F(s) being a Lambertian function describing the
angular dependence of light emerging from mucosal layer, L
a parameter representing the thickness of the mucosal
15 layer, and L a parameter representing the thickness of the
mucosal layer, and c, the concentration of hemoglobin,
which we find to be the main absorber relative to that of
collagen, which is responsible for light scattering.
Because both oxygenated and deoxygenated hemoglobin are
20 present, the total hemoglobin absorption is represented as
$\mu_a = (1-a)\mu_{(a)}^{(hb)} + a\mu_a^{(hbO_2)}$ with oxygen saturation parameter
$\alpha(0 \le \alpha \le 1)$.

Figure 5A shows the reflectance spectra from two
Barretts' esophagus tissue sites, both independently

-21-

diagnosed by standard pathological analysis to indicate (1)
normal and (2) precancerous (i.e. low grade dysplasia). As
can be seen, the differences in these unprocessed spectra
are small. To analyze them, Eq.(5) was first fit to the

5   broad features of the data by varying the parameters c, a
and L. As seen in Figure 5A, the resulting fits are quite
accurate. After removing this diffuse background structure
by calculating $R(\lambda)/\bar{R}(\lambda)$, the periodic fine structure is
seen in Figure 5B. Note that the fine structure from the

10 dysplastic tissue site exhibits higher frequency content
than that from the normal site. Equation (4) was then
employed to extract the respective nuclear size
distributions, yielding Figure 5C. The difference between
normal and dysplastic tissue sites is evident. The

15 distribution of nuclei from the dysplastic site is much
broader than that from the normal site and the peak
diameter is shifted from ~7 μm to about ~10 μm. In
addition, both the relative number of large nuclei (>10μm)
and the total number of nuclei are significantly increased.

20   Based on computer analysis, the uncertainty of the
above method in extracting nuclear size information is
estimated to be from 5% to 30%, depending on the noise
level and accuracy of the model. The distributions were
calculated using the same refractive index for both normal

25 and dysplastic nuclei. This is not entirely correct;
inasmuch as in stained histological sections dysplastic
nuclei appear hyperchromatic, which may be indicative of an

-22-

increase in refractive index. Thus, the relative number of
large nuclei in the distributions measured from dysplastic
sites may be slightly overestimated.

The ability to measure nuclear size distribution *in
vivo* has valuable applications in clinical medicine.
Enlarged nuclei are primary indicators of cancer, dysplasia
and cell regeneration. In addition, measurement of nuclei
of different size can provide information about the
presence of particular cells, and can thus serve, for
example, as an indicator of inflammatory response of
biological tissue. This suggests that different
morphology/pathology in the mucosal layer gives rise to
distinct patterns of nuclear distributions.

The physical characteristics that have been found to
be useful to differentiate between Barrett's non-dysplastic
and dysplastic epithelium were the total number of nuclei
and the percentage of large nuclei ($l > 10$ μm). A
comparison of pathological analysis of samples with the
optical analysis thereof provided the plot (total number of
nuclei vs. percentage of nuclei with a diameter large that
10 μm) in Figure 6. From those 50 sites, the cumulative
sensitivity and specificity, for this analysis were 83% and
100% respectively. The study had a positive predictive
value is 100%. The points indicated by n's were either
normal or inflamed and those indicated by d's were
displastic. A percentage in the range of 20-30% was found

-23-

to be an accurate diagnostic for this type, with 25% being
used in this particular example.

A preferred embodiment of a spectrograph system 300
employed for the collection of backscattered spectral data
5 from excised tissue samples using a spectrograph and a
charge coupled device (CCD), CMOS or other integrated solid
state imaging array is illustrated in Figure 7.

System 300 can use a broadband light source or tunable
laser 314 for irradiating a sample 46. Source 314
10 generates a beam 316 which is directed by mirror 318
through focusing optics 320 to impinge on sample 46 mounted
on a scattering substrate 325 and behind a transparent
window 321. The beam was focused on the sample at an angle
of incidence. The collection angle 330 can be determined
15 by an aperture or collimator 340 and is between 2 and 12
degrees, preferably between 3 and 8 degrees.

A portion of the scattered light 322 emitted by sample
46 was collected by collecting optics 324 a small angle
relative to the incident light. In another preferred
20 embodiment the angle of incidence and collection can be
along a single common axis. Collecting optics 324
collimates and F/matches the collected light for the
spectrograph 310. Prior to entering the entrance slit of
the spectrograph 310, the collected light was passed
25 through a series of filters 326 which attenuated the
unwanted scattered component of the collected light.

-24-

Figure 8 illustrates generally a process 400 for
collecting and analyzing the scattering spectrum from a
material of interest such as tissue. The method can be
performed both *in vitro* using a microscopy system or a
5   color imaging system as shown in Figure 7, or *in vivo* on a
patient. The illuminating light 402 from a source can use
radiation in the range of 300nm-1200nm, including the
infrared range. After collecting 404 and detecting 406
radiation, the diffuse background 408 can be removed and
10   the desired characteristics calculated 410. These results
can be used to provide a diagnosis of the region of
interest.

A preferred embodiment of the present invention
employs an analytical method based on data collection with
15   an optical fiber probe with fixed delivery and collection
geometry. Data analysis uses light diffusion, but rather
than directly apply the model to analyze tissue spectra, a
correspondence is established between the diffuse
reflectance spectra and a physical tissue representation
20   composed of scatterers and absorbers with known optical
properties. By analyzing spectra from this tissue model
using the analytical formulation, a calibration system is
provided which is simple to invert and accurately predicts
the concentrations of the scatterers and absorbers. Once
25   the calibration is established, the method is applied to
tissue spectra.

-25-

The following relates to the application of spectral
analysis to mucosal surfaces of tissues *in vivo*. In this
example adenomatous colon polyps are measured, which are
precursors of colon cancer. These polyps are a form of
5   colonic dysplasia and are histologically similar to
visually undetectable flat dysplasia, and are readily
detectable. The results are correlated with standard
histological examination, and can be used for early
detection of disease and, most importantly, exemplify how
10   this spectroscopic method can be applied *in vivo* to obtain
morphological and biochemical information.

Diffuse reflectance spectra were collected *in vivo*
from adenomatous polyps on 13 patients undergoing routine
colonoscopy. Data were collected simultaneously with
15   multi-excitation fluorescence spectra: a xenon-arc
flashlamp with 10 μs pulse duration and an average input
energy of 4Jj/pulse was used as white light source. An
imaging spectrograph dispersed the collected, light and a
gated diode array detector was employed for light detection
20   in the 360-685 nm spectral range. A 12 μsec gate
synchronized with the lamp pulse was used to minimize
background from endoscopic illumination. The detector was
controlled by a PC notebook computer, where the data were
transferred and stored.

25   Light was delivered and collected using an optical
fiber probe which was advanced through the accessory
channel of the colonoscope and brought into contact with

-26-

the tissue. The probe consisted of a central optical fiber
for light delivery, surrounded by six concentric fibers for
light collection. All fibers had 200 μm core diameter and
NA=0.22. The probe tip was fitted with a quartz shield

5 approximately 1.5 mm in length and diameter, which provided
a fixed delivery/collection geometry with uniform circular
delivery and collection spots in the form of overlapping
cones with approximate radii of r_d=0.35 mm and r_c=0.55 mm,
respectively. The tip was beveled at an angle of 17

10 degrees, to eliminate unwanted specular reflections from
the shield/air interface.

The diffuse reflectance spectrum of a 20% by volume
$BaSO_4$ powder suspension was used as a reference, to take
into account the spectral characteristics and overall

15 intensity of the xenon lamp. The probe was immersed in the
suspension and a reference diffuse reflectance spectrum was
recorded prior to collection of each data set. Tissue
spectra were calibrated by dividing by this reference
spectrum. Diffuse reflectance spectra were measured from a

20 few different sites on every adenomatous polyp and from
corresponding sites in the surrounding normal mucosa.
Single-pulse excitation was used in order to avoid motional
artifacts. The polyps were than removed and examined
histologically, while the normal mucosa sites were not

25 biopsied.

To represent diffuse reflectance, biological tissue
was approximated as being a homogeneous semi-infinite

-27-

turbid medium with reduced scattering and absorption
coefficients μ_s' (λ) and μ_a' (λ), respectively (λ is the
wavelength of light). Part of the incident light is
absorbed in the tissue, while the non-absorbed part is
5 subject to multiple scattering and eventually emerges from
the surface as diffuse reflectance. A certain fraction of
this return light is collected by the probe, while the
remaining part escapes undetected. The amount of the light
collected depends on the optical properties μ_s' (λ) and μ_a'
10 (λ), as well as on the probe diameter, r_p. Because r_p is
finite, it serves as a scale length, enabling μ_s' (λ) and
μ_a' (λ) to be determined separately.

     To characterize light collection by an optical probe,
knowledge of the spatial and angular resolution of the
15 diffuse reflectance on the surface of the tissue is
required. Using the method of images to implement the
diffusion approximation to the radiative transfer equation
the diffuse reflectance radial density, R (λ, r), at a
distance r from the point of incidence of the light on the
20 surface of a semi-infinite turbid medium is given by

$$R(\lambda,r) = \frac{z_0\mu_s'}{4\pi\mu_s' + \mu_s}\left\{(\mu+\frac{l}{r_1})\frac{e^{-\mu r_1}}{r_1^2} \div (1+\frac{4}{3}A)(\mu+\frac{1}{r_2})\frac{e^{-\mu r_2}}{r_2^2}\right\}, \tag{6}$$

where $\mu = (3\mu_a(\mu_a - \mu_s'))^{1/2}, z_0 \frac{1}{\mu_s' + \mu_a}$

and $r_1 = \left(z_0^2 + r^2\right)^{1/2}, r_2 = \left(z_0^2(1+\frac{2}{3}A)^2 + r^2\right)^{1/2}$

-28-

The parameter A depends on the refractive index n of the medium (A=1 for n=1 and A>1 for n>1). A reasonable assumption for the average refractive index of colon tissue is n≅ 1.4 so that A ≅ 3.2.

5   To find the total light collected by the probe, Eq. 6 must be integrated over the spatial extend of the delivery and collection areas, characterized by radii r_d and r_c, respectively. Assuming the incident light intensity to be uniform over the entire delivery area, the diffuse

10   reflectance R_p (λ) collected by the probe is given by

$$R_p(\lambda) = \frac{1}{r_d^2} \int_0^{r_c} r dr \int_0^{2\pi} d\phi \int_0^{r_d} R(\lambda, \bar{r} - \bar{r}') r' dr' , \qquad (7)$$

with $|\bar{r} - \bar{r}'| = (r^2 + r'^2 - 2rr' \cos\Phi)^{1/2}$. The integrals is Eq. 7 can be evaluated numerically. However, to obtain a simple analytical expression for R_p (λ), we assume point delivery

15   of light (r_d = 0) and collection over a circular spot of radium r_c, we then obtain:

$$R_p(\lambda) = 2\pi \int_0^{r_c} R(r) r dr$$

-29-

$$= \frac{\mu_s'}{\mu_s' \div \mu_a} \left\{ e^{-uz_o} \times e^{-\left(1+\frac{1}{3}A\right)uz_o} - z_o \frac{e^{-ur'}}{r_1'} - (1+\frac{4}{3}A)z_o \frac{e^{-\mu r_2'}}{r_2'} \right\} \tag{8}$$

with $r_2' = \left(z_o^2 + r_c^2\right)^{1/2}, r_2' = \left(z_o^2\left(1+\frac{2}{3}A\right)^2 + r_c^2\right)^{1/2}$

The optimal value of r_c was found by calibrating Eq. 8 on physical tissue models with known optical properties. The

5   advantage of using Eq. 8 is that it is much easier to invert than Eq. 7, which requires numerical integration. Eq. 8 gives the diffuse reflectance at the perpendicular direction to the tissue surface. This is acceptable because light is only collected by the optical probe at

10 directions with a maximum deviation of approximately 10 degrees from the direction perpendicular to the surface.

Eq. 8 can be used to analyze the diffuse reflectance spectra collected by the probe. From these measurements of the tissue spectra, hemoglobin is the only significant

15 light absorber in colon tissue in the visible range of the spectrum, and is encountered in both oxygenated and deoxygenated forms. The light absorption properties of both forms have been studied and their molar extinction coefficient spectra e_{HbO2} (λ), e_{Hb} (λ) are shown in Figure 9.

20 Oxyhemoglobin absorption presents a maximum at 415 nm and two secondary maxima at 542 and 577 nm, while deoxyhemoglobin has a maximum at 430 nm and only one

-30-

secondary maximum at 555 nm. The total absorption

coefficient, μ_j (λ) is given by

$$\mu_u(\lambda) = 2.3 C'_{hb}\left(\alpha \varepsilon_{hb0_2}(\lambda) + (1-\alpha)\varepsilon_{hb}(\lambda)\right) \quad , \tag{9}$$

where $\alpha = \dfrac{C_{hb0_2}}{C_{hb0_2} + C_{hb}}$ is the Hb oxygen saturation parameter,

5   C_{hb0_2} and C_{Hb} are the concentrations of oxy and deoxy Hb,

respectively, and C'_{hb} = C_{hbo2} + C_{Hb} the total concentration

of HB.

Determination of C_{Hb} and α was performed in the

following way. For a given tissue spectrum, $R_p(\lambda)$, initial

10   values were assigned (typically C_{Hb} = 0.0 and α = 0.5).

Eq. 8 was then numerically inverted to find μ_s' (λ), which

exhibited residual spectral features of HB absorption. The

parameters C_{Hb} and α were then modified, and the process

was repeated recursively until μ_s' (λ) exhibited a smooth

15   spectral shape with the Hb spectral features absent. In

this way, μ_s' (λ) was simultaneously determined with C_{Hb} and

α.

Table 2

Model Parameter	Normal	Adenomatous Polyp

-31-

Total Hb Concentration C_{Hb} (mg/dL)	13.6 ± 8.8	72.0 ± 29.2
Hb Oxygen Saturation α	0.59 ± 0.08	0.63 ± 0.10
Effective Scatterer Density ρ_s (x10^8 mm^{-3})	9.2 ± 7.5	3.5 ± 4.0
Effective Scatterer Size d_s (mm)	0.56 ± 0.18	0.94 ± 0.44

15   The above procedure is based on the assumption that
$\mu_s{}'(\lambda)$ is a relatively smooth function of the wavelength
λ, which analysis confirms, as will become evident from the
discussion below. In general, $\mu_s{}'(\lambda)$ is the sum of
contributions from the various tissue scatterers.
20 Unfortunately, detailed information about these individual
scatterers is not available. Therefore, $\mu_s{}'(\lambda)$ was
written as

$$\mu_s'(\lambda) = \rho_s \sigma'(\lambda), \qquad\qquad\qquad (10)$$

-32-

with ρ_s the *effective* scattering density and σ' (λ) the

effective reduced scattering cross section, i.e. the tissue

scattering properties are modeled in an average way, as if

tissue contained a single well-defined type of scatterer.

5   In general, σ' (λ) depends on the refractive index, shape

and size of the scatterer, as well as on the refractive

index of the surrounding medium. For a spherical scatterer

with diameter d_s, σ' (λ) can be calculated numerically

using Mie scattering theory.

10   Figure 10 shows such a calculation of σ' (λ). Note

that the slope of σ' (λ) depends on d_s in a simple way i.e.

the slope is inversely related to scatterer size. In this

way it was possible to assign a scatterer size to every σ'

(λ) and hence to every μ_s' (λ) in the range d_s = 0.2-2.0

15 μm. For example, by inspecting μ_s' (λ) of normal colon

mucosa, previously reported based on *in vitro* measurements,

it can be seen that they correspond to a scatterer size d_s

$\cong 0.35$ μm. Once d_s was determined, the density p_s was by

dividing μ_s' (λ) by σ' (λ). In summary, for each tissue

20 diffuse reflectance spectrum four parameters were obtained,

C_{Hb}, α, p_s and d_s.

In calculating the results shown in Figure 10, the

scatterer and the surrounding medium refractive indices

were assumed similar to those likely to be found in tissue.

25 Reasonable approximations are a refractive index of

approximately 1.4 for the scatterers and 1.36 for the

surrounding medium. These values can be justified by

-33-

noting that the lower bound for the tissue refractive index
is set by the refractive index of water, which is
approximately equal to 1.33 in the visible range, and the
upper bound is set by the maximum refractive index reported
5   for soft tissue, which is around 1.45. Such values are
consistent with those generally observed for soft
biological tissues.

The physical tissue representation served as a method
for confirming the applicability of the various
10 approximations made in developing Eq. 8. The samples
consisted of mixtures of spherical microparticles with Hb
in various concentrations. The model established that
these mixtures simulated the optical properties of tissue
samples. In addition, the range of validity of the
15 analytical model in terms of the optical properties was
established, and the optimal value for the parameter r_c,
Eq. 8. was determined.

Polystyrene bead suspensions in de-ionized water
(Polysciences, Inc.) were used to simulate tissue light
20 scattering, and Hb solutions prepared from lyophilized
human Hb (Sigma, H0267) were used to stimulate absorption.
The scattering properties of the beads were calculated
using Mie theory. The bead diameter was 1.07 μm, and the
refractive index n_p of polystyrene was given by the
25 expression of $n_p = 15607 + 10002/\lambda^2$ (26), (λ in nm), and
the polystyrene concentration was 0.625% by volume. The
reduced scattering coefficient varied from approximately

-34-

1.7 mm^{-1} at 400 nm. This spectral dependence is similar to that shown in Figure 10 with d_s = 1.0 μm, with the difference that the slope is larger due to the larger refractive index of polystyrene.

5   Since light absorption by polystyrene is negligible in the visible range, absorption was solely due to oxyhemoglobin. The size of the physical-tissue model was approximately 3x3x0.5 cm, simulating the flat geometry of normal colon mucosa. Additional geometries were

10   investigated such as a cylindrical geometry with 1 cm depth and 0.5 cm diameter, to simulate the geometry of the polyps, but no significant spectral differences were found. The range of optical parameters used was chosen based on the previously reported independent measurements of colon

15   tissue optical parameters performed *in vitro*.

        Figure 11 shows diffuse reflectance spectra measured on the physical tissue model with various concentrations of Hb vs. the analytical model predictions, which were obtained by setting r_c = 0.45 mm in Eq. 3. This was

20   determined to be the optimal value for r_c, which was kept fixed throughout the entire data analysis. It was also found that the parameter $Z_0 = 1/(0.6\mu_d + \mu_s')$ improved the agreement between the analytical model and the physical tissue model data, especially for large values of

25   absorption. The physical tissue model spectra shown in Figure 11 are very similar to the tissue spectra presented below. This fact serves as indirect confirmation of the

-35-

assumptions made in developing the model, regarding tissue scatterers (modeled as microspheres) and tissue absorption (attributed to Hb).

5   The analytical model was found to accurately predict the physical tissue model spectra for Hb concentrations in the physiological range of interest. For Hb concentrations lower than 100 mg/dL, the deviation between the two models was always smaller than 10% over the entire wavelength range. The largest deviation occurred when absorption

10   became comparable to scattering. This is shown in curve (d) of Figure 11, near the peak of Hb absorption, around 415 nm. The Hb concentration was in this case 250 mg/dL which corresponds to an absorption coefficient of approximately 5 mm^{-1} at 415 nm, while the scattering

15   coefficient was approximately 2.8 mm^{-1} at the same wavelength.

Figure 12 shows typical diffuse reflectance spectra from one adenomatous polyp site and one normal mucosa site. Significant spectral differences are readily observable,

20   especially in the blue region of the spectrum, where the Hb absorption valley around 420 nm is the prominent spectral feature. This valley is much more prominent int he polyp spectrum, which also shows a continuous decrease in intensity starting from the red end (~700 nm) and moving

25   toward the green region (~500 nm) of the spectrum, while in the same range the normal mucosa spectrum shows a steady increase in intensity. The secondary absorption dips of

-36-

oxyhemoglobin (542 and 577 nm) are much more prominent in
the adenomatous polyp spectrum, indicating increased Hb
concentration. According to the model analysis the normal
mucosa spectrum was characterized by Hb concentration C_{Hb} =
5   22.5 mg/dL, while the corresponding value for the
adenomatous polyp was about 6 times higher (C_{Hb} = 165
mg/dL). The Hb saturation was found to be 0.65 $\pm$ 0.05, and
0.55 $\pm$ 0.05 respectively.

Figure 13 shows the scattering spectra μ_s' (λ)
10   calculated from the data shown in Figure 12, along with the
best Mie theory fits. The main difference between the
spectra of the two tissue types is observed in the spectral
slope, which corresponds to different effective scattering
sizes, d_s = 1.5 μm for the polyp and d_s = 0.35 μm for
15   normal mucosa. The values for the scatterer densities were
found to be p_s = 15x10^8 mm^{-3} for the normal mucosa, and p_s =
1.3x10^8 mm^{-3} for the adenomatous polyp. Figure 12 also
shows the best analytical model fits to the data, using Eq.
8. The model accurately describes the data, despite the
20   dramatic differences noted in the spectral shape between
the two tissue types and the fact that μ_s' (λ) is
approximated assuming a homogeneous distribution of
spherical scatterers. The deviation between the data and
the model in typically smaller than 10% for most of the
25   wavelength range.

Figures 14A-14D shows the calculated values of the
four parameters for all tissue sites studied: (A) total Hb

-37-

concentration C_{Hb} (B) Hb oxygen saturation α, (C) effective
scatterer density p_s and (D) effectiveness scatterer size
d_s. Adenomatous polyps were clearly characterized by
increased Hb concentration, while there were no observable
5 differences in terms of the Hb oxygen saturation. The
effective scatterer density was in general lower in
adenomatous polyps, and the effective scatterer size
larger, even though there was significant overlap of these
parameter distributions between the two tissue types.
10 Table 2 summarizes the results shown in Figures 14A-14D by
giving the average values and the standard deviations for
each parameter.

Figure 15 shows a plot of the Hb concentration C_{Hb},
vs. the effective scatterer size d_s. These two parameters
15 are shown together in order to summarize and illustrate the
differences found in the scattering and absorption
properties of normal mucosa and adenomatous polyps in the
colon. Note that the normal mucosa data tend to form a
cluster, while the adenomatous polyp data are separated,
20 and characterized by a wider spread and irregular
distribution, in both the effective scatterer size and the
Hb concentration.

A methodology has been described which provides
quantitative information about colon mucosal tissues *in*
25 *vivo*, based on diffuse reflectance measurements. The main
components of this methodology are (a) data collection
through an optical fiber probe with a fixed

-38-

delivery/collection geometry, (b) an analytical model for
data analysis based on light diffusion, and (c) a physical
tissue model for calibration of the analytical model.

The use of an optical probe with fixed geometry
5 enables consistent data collection, and independent
determination of the scattering and absorption. Modeling
of the probe geometry is facilitated through the use of the
parameter r_c, which also defined the probe's sensitivity to
absorption. A probe with large r_c will render the spectra
10 collected more sensitive to tissue absorption as compared
to a probe with a smaller r_c. In Figure 4, the secondary
Hb absorption peaks are barely noticeable in the normal
mucosa spectrum: a probe with larger r_c would make these
features more prominent.

15 The analytical diffusion theory model is amenable to
numerical inversion and successfully describes the tissue
data after calibration on the physical tissuemodel composed
of polystyrene beads and oxy hemoglobin. Other researchers
have already used variants of the analytical model
20 described here, in the study of diffuse reflectance from
tissues and physical tissue models in the IR range. The
present study is, to our knowledge, the first to apply the
model in the visible range, to *in vivo* data from human
mucosal tissue, measured with an optical fiber probe. By
25 working in the visible rather than in the IR, light
penetration was restricted to approximately 0.5 mm, i.e.
the mucosa layer where precancerous changes occur. Using

-39-

the model, we have shown that it is possible to obtain
quantitative information about the tissue studied, such as
Hb concentration, Hb oxygen saturation, effective scatterer
size, and effective scatterer density. The results show
5   that diffuse reflectance provides a tool for quantitative
analysis of mucosal tissue surfaces *in vivo.*

'   The basic approximation made in the model is that Hb
is the only significant absorber in colon mucosa in the
visible range of the spectrum. Even though this assumption
10   lacks direct confirmation, the fact that the data strongly
exhibit the characteristic features of Hb absorption,
clearly indicates that Hb is a major absorber. In
addition, the spectra measured on the tissue physical
model, in which Hb was the only absorber, closely resemble
15   the tissue spectra.

In a similar way, tissue scattering was modeled as due
to homogeneous spherical scatterers with known refractive
index. The approximation permits a quantitative
characterization in terms of two basic parameters, the
20   effective scatterer size and the effective scatterer
density. These parameters provide an estimate of the
average scattering properties. The fact that the spectra
measured on physical tissue models reproduce the actual
tissue spectra, serves again (as in the case of Hb), as an
25   indirect confirmation of the validity of this
approximation.

-40-

Data analysis showed that adenomatous colon polyps
were characterized by increased Hb concentration. It is
known that tumors and cancerous tissues exhibit increased
microvasculature, and hence increased blood content. Using
5   morphometry and vascular casting in combination with
scanning electron microscopy techniques. Precancerous
tissues such as adenomatous polyps of the colon are also
characterized by increased microvascular volume the above
in agreement with these reports in terms of observing the
10   increased Hb concentration. Others report increased
microvascularity of the colon mucosa associated with
Crohn's disease and ulcerative colitis. Even though we did
not study these tissue types, the technique employed here
could prove useful for the *in vivo* study of such diseases.
15   The Hb oxygen saturation was found to be approximately
60%, on average, for both normal mucosa and adenomatous
polyps. This result is reasonable, because the
measurements were essentially performed in the capillary
network of the mucosa, where oxygen is transferred from Hb
20   to tissue. Hb oxygen saturation drops within the
capillaries from approximately 97% (arterial blood) to
about 40% (venous blood) with the measured values (around
60-70%) appropriately placed int he middle of this range.
The fact that there were no differences observed between
25   the two tissue types, can probably be attributed to the
fact that adenomatous polyp metabolism is not significantly
altered, so as to introduce changes in Hb oxygenation,

-41-

which is probably related to the disturbed metabolism of
such tissues. The technique presented here could be used
in vivo for the study of tumors on the surfaces of hollow
organs, or for the study of other tissue types when
5 knowledge of Hb saturation is needed.

An intrinsic differentiation in the scattering
properties between the two tissue types was observed. For
adenomatous polyps, the average effective scattering size
was larger, and the average effective scatterer density was
10 smaller, as compared to normal mucosa. There are a number
of hypotheses identifying contributions to scattering from
various microstructures, .both extracellular such as
collagen fibers, and intracellular such as mitochondria and
cell nuclei. One model provides contributions to light
15 scattering from intracellular structures is increased in
adenomatous polyps because cells occupy a higher volume
ratio. In addition, the submucosa, in which collagen is
more densely packed is usually located too far away from
the polyp surface in order to be able to contribute to
20 light scattering. This can explain the lower scatterer
density in adenomatous polyps, provided that intracellular
scatterers are larger than extracellular ones, on average.

EQUIVALENTS

While this invention has been particularly shown and
25 described with reference to preferred embodiments thereof,
it will be understood by those skilled in the art that

-42-

various changes in form and details may be made therein
without departing from the spirit and scope of the
invention as defined by the appended claims. Those skilled
in the art will recognize or be able to ascertain using no

5 more than routine experimentation, many equivalents to the
specific embodiments of the invention described
specifically herein. Such equivalents are intended to be
encompassed in the scope of the claims.

-43-

CLAIMS

What is claimed is:

1. A method of measuring a size of a structure in a layer
    of tissue comprising:
5   directing radiation onto a region of interest in
    the layer of tissue;
            collecting radiation from the tissue;
            detecting the collected radiation; and
            determining a size of a structure within the
10 tissue layer.

2. The method of Claim 1 further comprising determining
    if the region of interest includes dysplastic tissue.

3. The method of Claim 1 further comprising directing
    radiation onto the tissue using a fiber optic probe.

15 4. The method of Claim 1 further comprising collecting
    the radiation from the tissue with a fiber optic
    probe.

5. The method of Claim 1 further comprising determining
    an average nuclear size of nuclei within the region of
20 interest.

-44-

6.   The method of Claim 1 further comprising measuring a
      diameter of a tissue nucleus within the region of
      interest.

7.   The method of Claim 1 further comprising measuring a
5   periodic component of an intensity of radiation from
      the tissue as a function of wavelength.

8.   The method of Claim 7 further comprising determining
      the size of a nucleus in the tissue from the periodic
      component.

10 9.   A method of optically measuring tissue comprising:
            directing radiation onto a region of interest in
      tissue to be measured;
            collecting radiation from the tissue; and
            measuring a periodic component of collected
15   radiation as a function of wavelength to determine a
      physical characteristic of the tissue.

10.   The method of Claim 9 further comprising determining
      if the region of interest includes dysplastic tissue.

20 11.   The method of Claim 9 further comprising directing
      radiation onto the tissue using a fiber optic probe.

-45-

12.   The method of Claim 9 further comprising collecting
      the radiation from the tissue with a fiber optic
      probe.

13.   The method of Claim 9 further comprising determining
5   an average nuclear size of nuclei within the region of
      interest.

14.   The method of Claim 9 further comprising measuring a
      diameter of a tissue nucleus within the region of
      interest.

10 15.   The method of Claim 9 further comprising collecting
      radiation with an endoscope, the endoscope having an
      imaging sensor at a distal end of the endoscope.

16.   The method of Claim 9 further comprising determining a
      density of nuclei in the tissue from the periodic
15   component.

17.   A method of determining a presence of dysplasia in
      tissue comprising:
           directing radiation onto a region of interest in
      an epithelial layer of tissue;
20   collecting backscattered radiation from the
      tissue;

-46-

detecting the collected radiation with a
detector; and

determining the presence of dysplasia in the
region of interest of the tissue.

18.   The method of Claim 17 further comprising determining
        if the region of interest includes dysplastic tissue.

19.   The method of Claim 17 further comprising collecting
        radiation in the range of 350 nm to 700 nm.

20.   The method of Claim 17 further comprising collecting
        the radiation from the tissue with a fiber optic
        probe.

21.   The method of Claim 17 further comprising determining
        an average nuclear size of nuclei within the region of
        interest.

22.   The method of Claim 17 further comprising measuring a
        diameter of a tissue nucleus within the region of
        interest.

23.   The method of Claim 1 further comprising measuring a
        periodic component of an intensity of radiation from
        the tissue as a function of wavelength.

-47-

24. The method of Claim 7 further comprising determining
the size of a nucleus in the tissue from the periodic
component.

25. A method of optically measuring a material comprising:
5   directing radiation onto a region of interest in
the material tissue to be measured;
           collecting radiation from the material;
           detecting a scattering spectrum from the
collected radiation; and
10   measuring a periodic component of collected
radiation as a function of wavelength to determine a
physical characteristic of the material.

26. The method of Claim 25 further comprising directing
15   radiation onto the material using a fiber optic probe.

27. The method of Claim 25 further comprising collecting
the radiation from the material with a fiber optic
probe, the probe having an optical fiber with a
numerical aperture in a range of 0.05-0.25.

20 28. The method of Claim 25 further comprising determining
an average nuclear size of nuclei within the region of
interest.

-48-

29.   The method of Claim 25 further comprising measuring a
      number of particles per unit area within the region of
      interest.

30.   An apparatus for optically measuring tissue
5   comprising:
           a radiation source that illuminates a region of
      interest in tissue to be measured;
           an optical system that collects radiation from
      the tissue;
10   a detector system that senses the collected
      radiation; and
           a data processor that determines a periodic
      component of detected radiation as a function of
      wavelength to determine a physical characteristic of
15   the tissue.

31.   The apparatus of Claim 30 further comprising a
      broadband light source that generates light in a range
      of 350-700 nm.

20 32.   The apparatus of Claim 30 further comprising a fiber
      optic probe that couples the source to the tissue.

33.   The apparatus of Claim 30 further comprising a fiber
      optic probe that collects the light in a collection
      angle between 2 and 12 degrees.

-49-

34. The apparatus of Claim 33 wherein the probe is
     insertable in an endoscope.

FIG. I
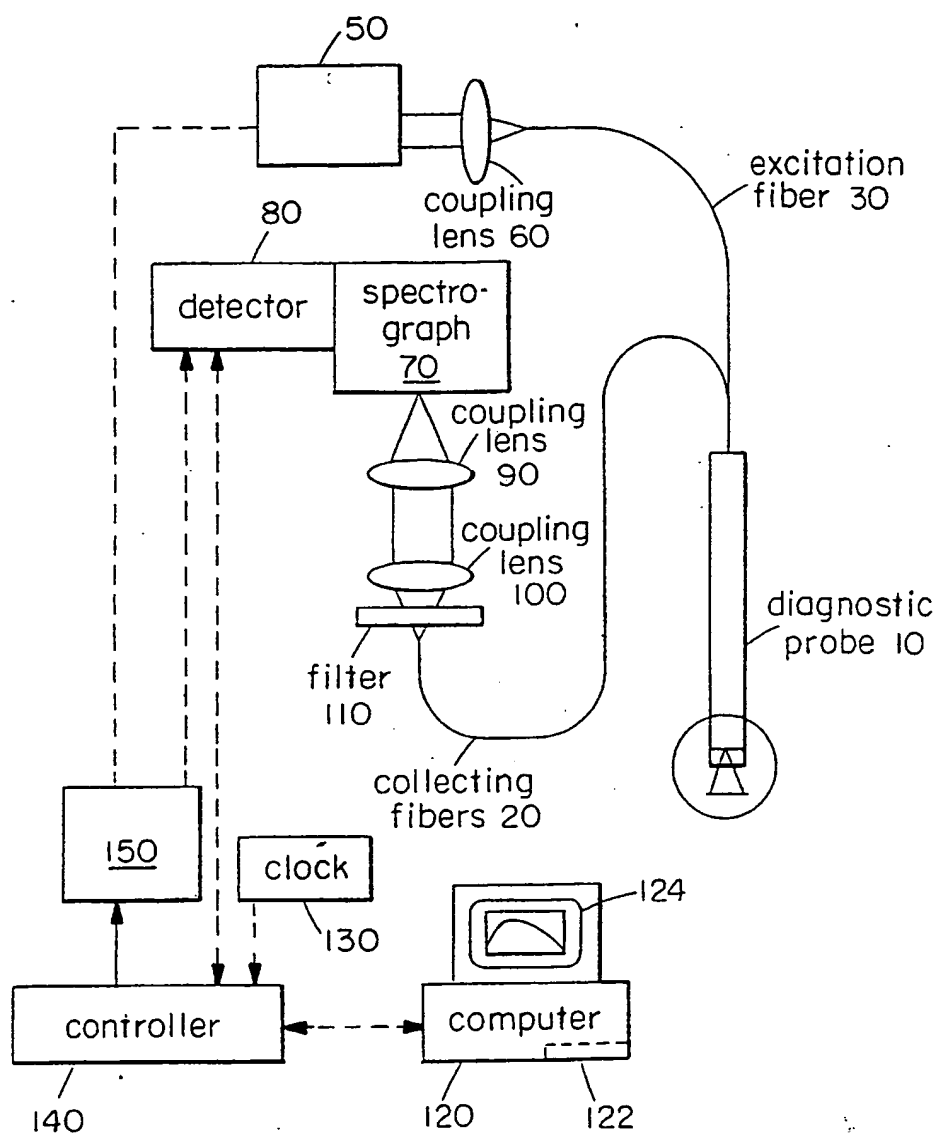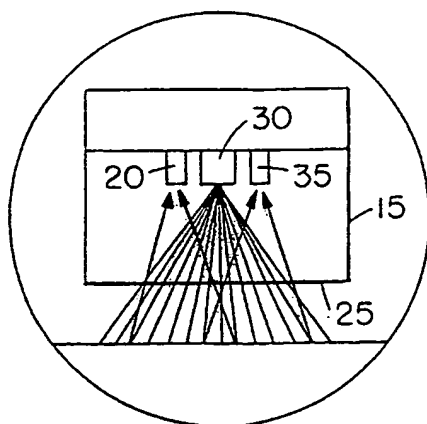
FIG 2

This Page Blank (uspto)
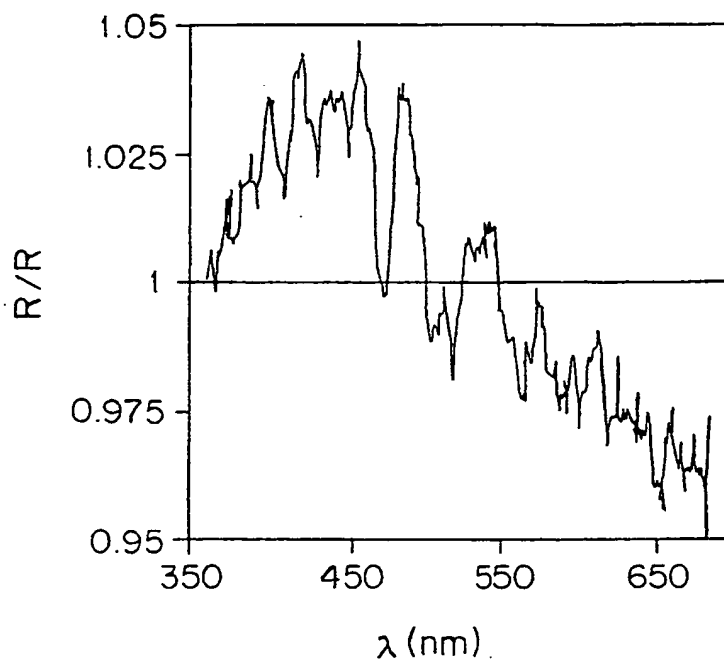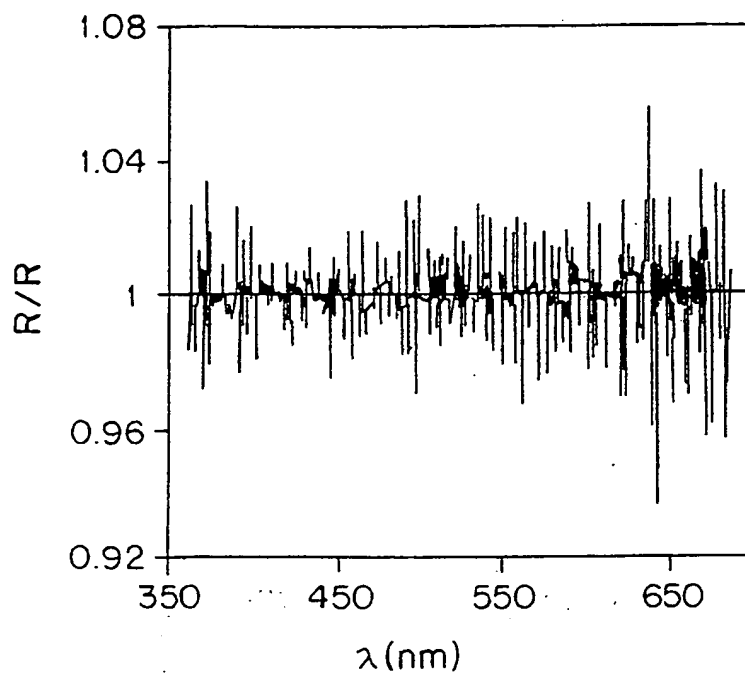
FIG. 3A
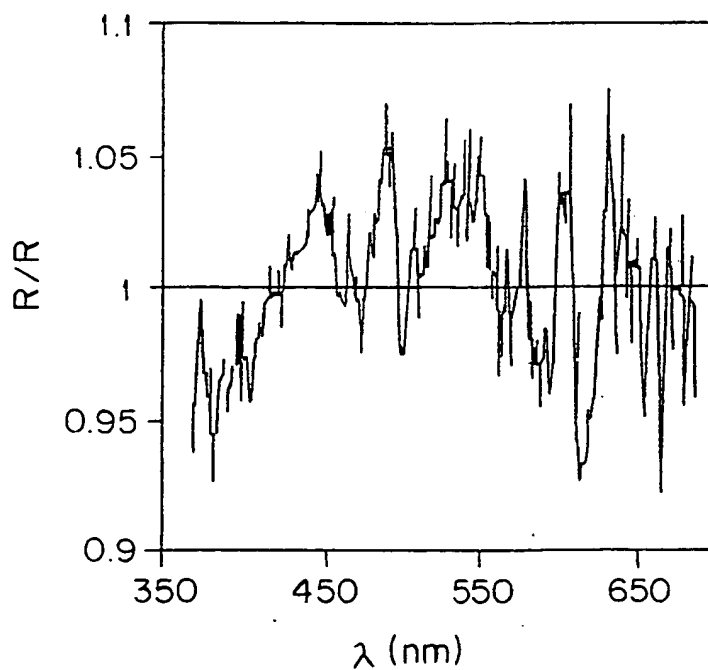
FIG. 3B

This Page Blank (uspto)

FIG. 3C
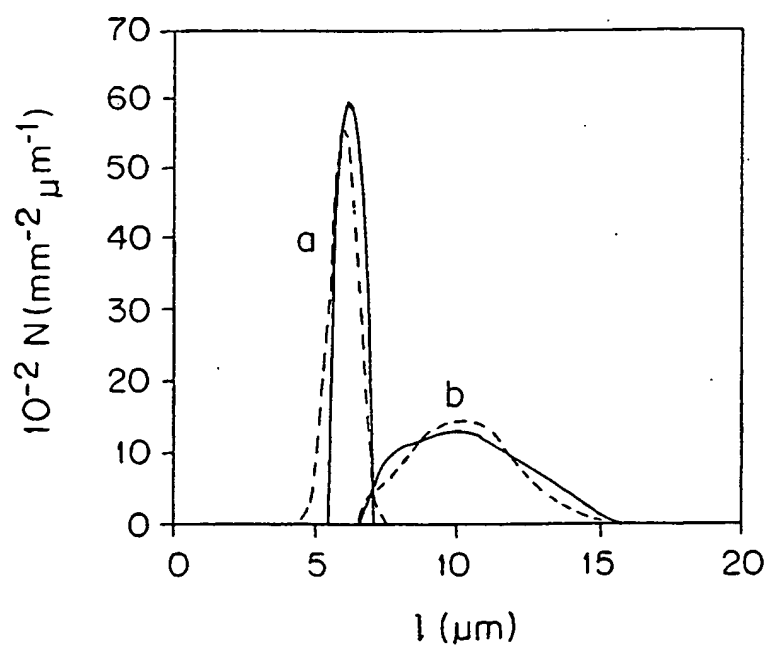

FIG. 4

This Page Blank (uspto)
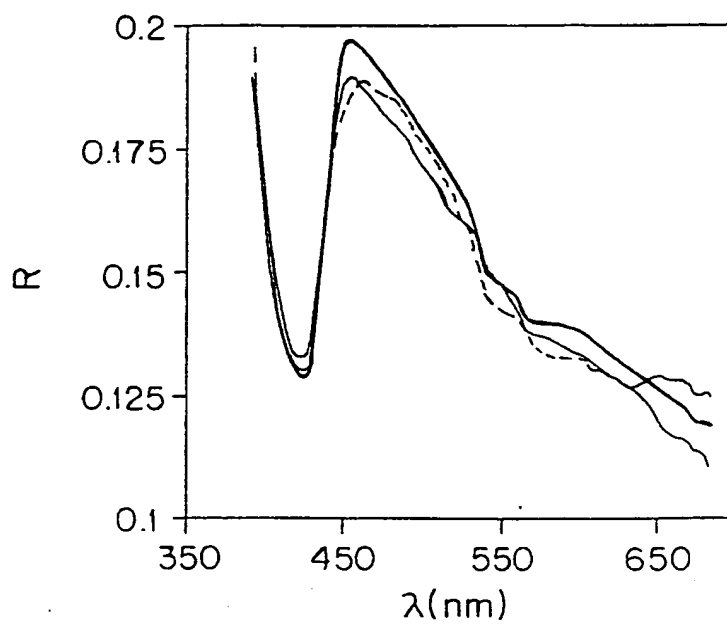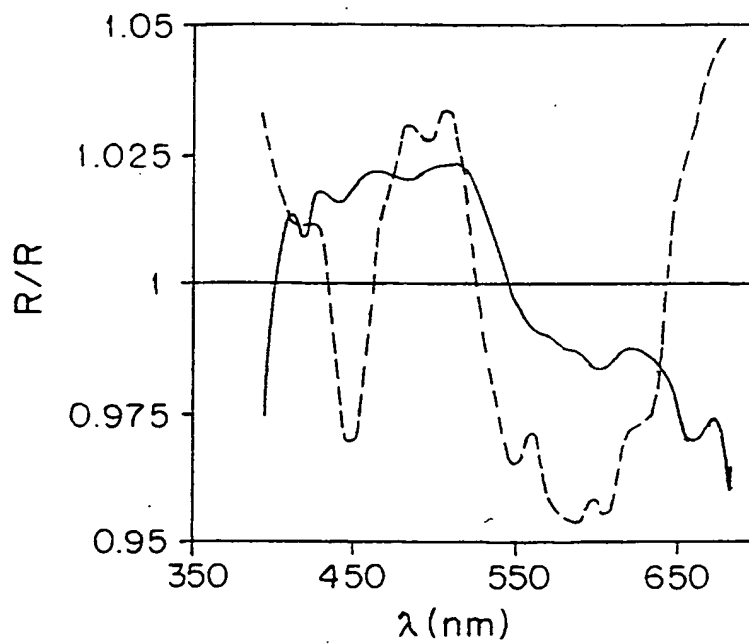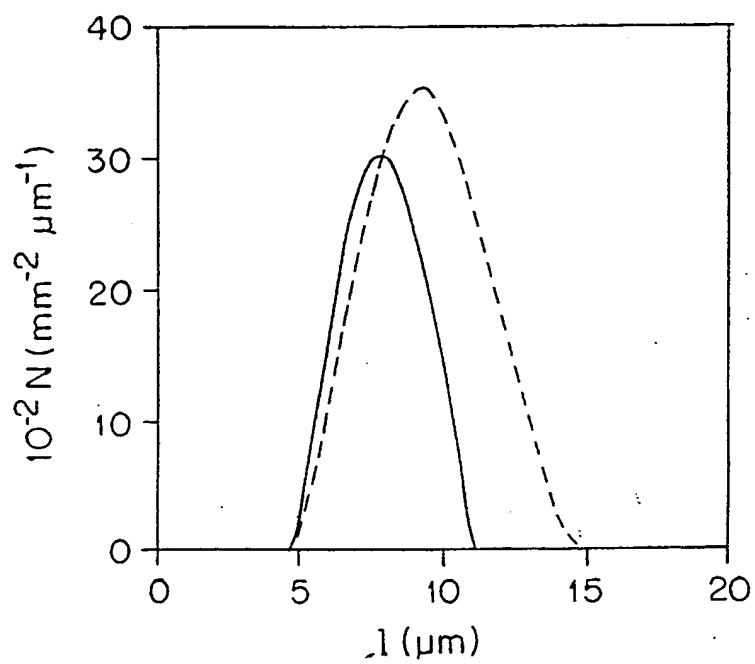
FIG. 5A

FIG. 5B

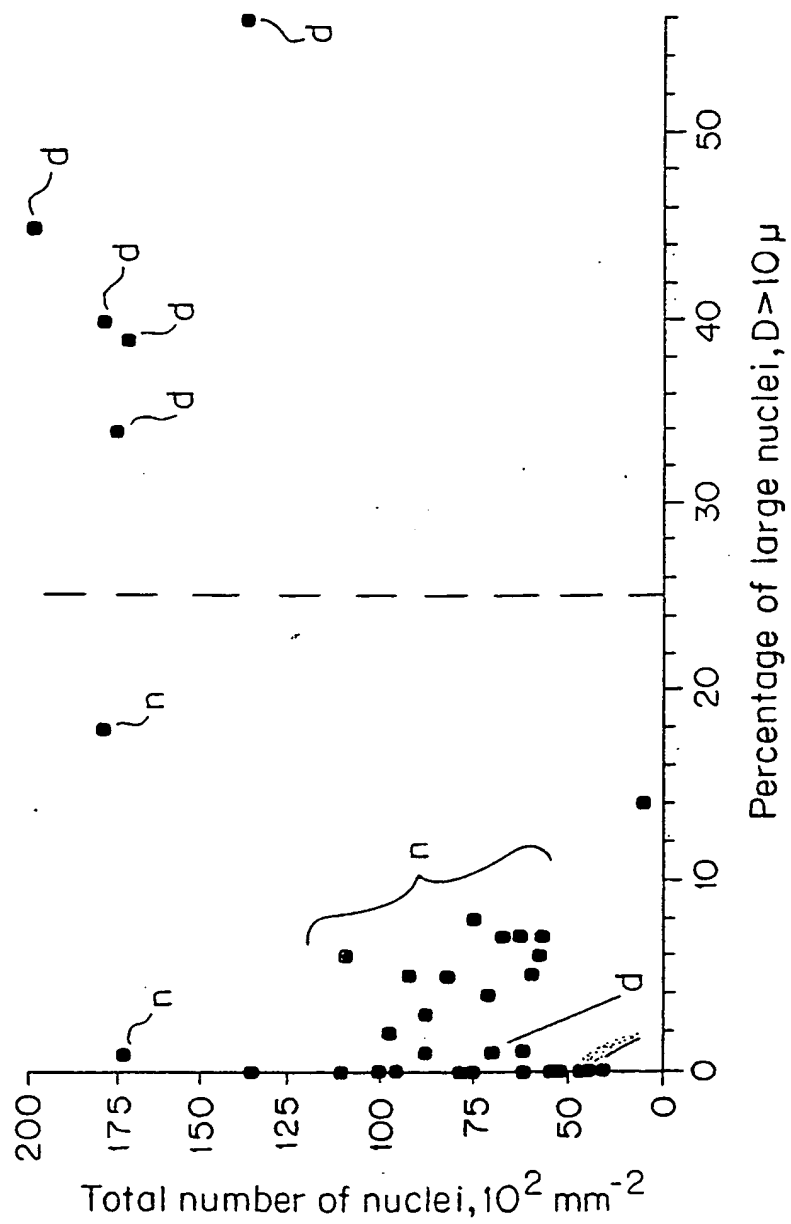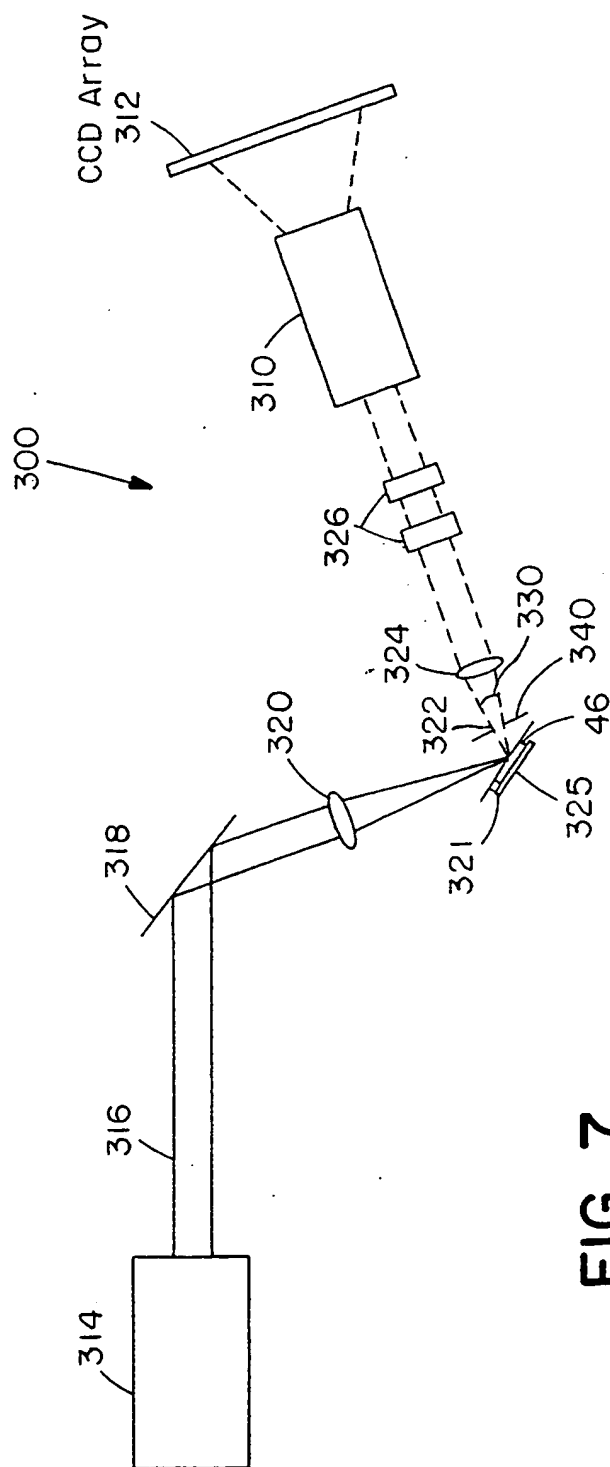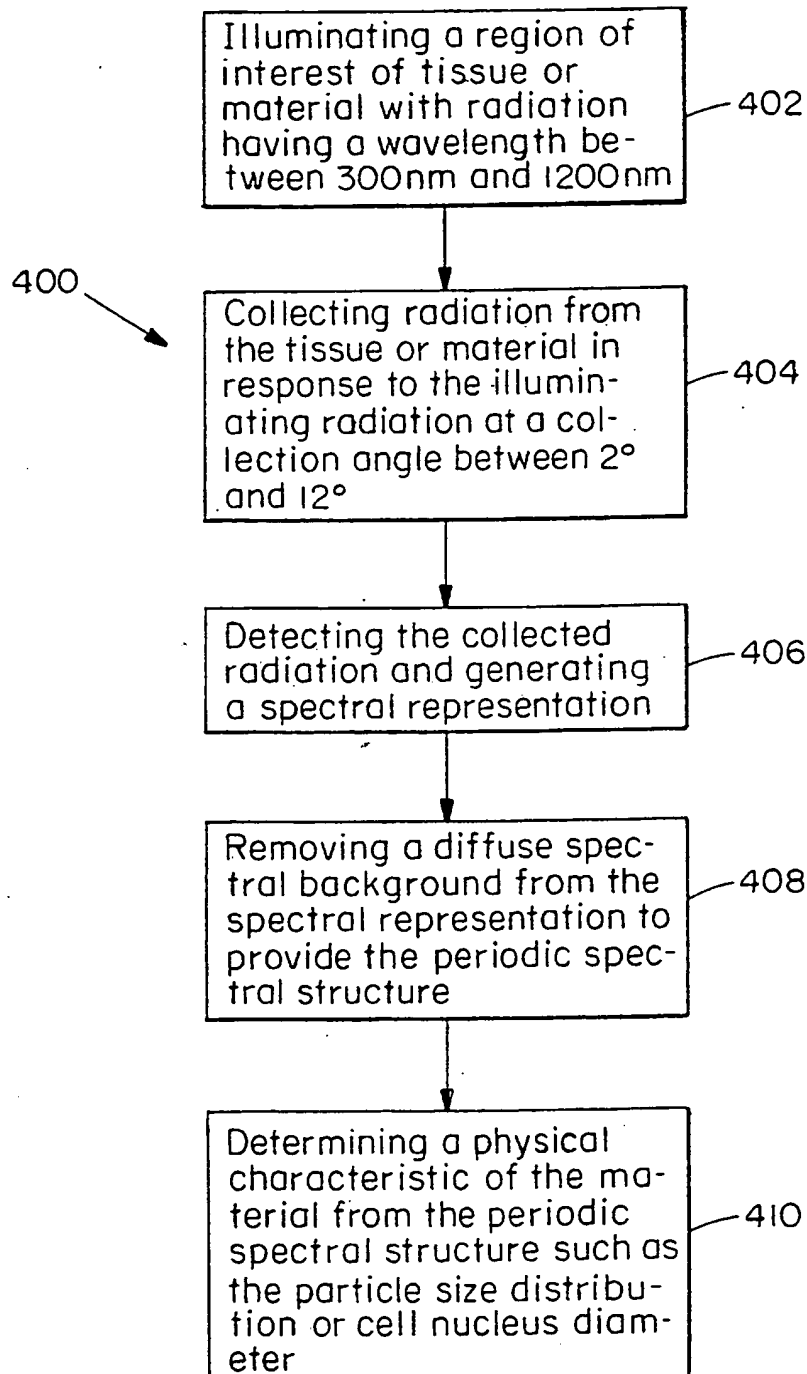This Page Blank (uspto)

FIG. 5C

This Page Blank (uspto)

FIG. 6

This Page Blank (uspto)

CCD Array
312

310

300

326

324
330
340

320
322

318
316
321
325
46

314

FIG. 7

This Page Blank (uspto)

400

```
┌─────────────────────────┐
│ Illuminating a region of│
│ interest of tissue or   │
│ material with radiation │─── 402
│ having a wavelength be-  │
│ tween 300nm and 1200nm  │
└─────────────────────────┘
            │
            ▼
┌─────────────────────────┐
│ Collecting radiation from│
│ the tissue or material in│
│ response to the illumin- │─── 404
│ ating radiation at a col-│
│ lection angle between 2° │
│ and 12°                 │
└─────────────────────────┘
            │
            ▼
┌─────────────────────────┐
│ Detecting the collected │
│ radiation and generating│─── 406
│ a spectral representation│
└─────────────────────────┘
            │
            ▼
┌─────────────────────────┐
│ Removing a diffuse spec- │
│ tral background from the │
│ spectral representation to│─── 408
│ provide the periodic spec-│
│ tral structure          │
└─────────────────────────┘
            │
            ▼
┌─────────────────────────┐
│ Determining a physical  │
│ characteristic of the ma-│
│ terial from the periodic │─── 410
│ spectral structure such as│
│ the particle size distribu-│
│ tion or cell nucleus diam-│
│ eter                    │
└─────────────────────────┘
```
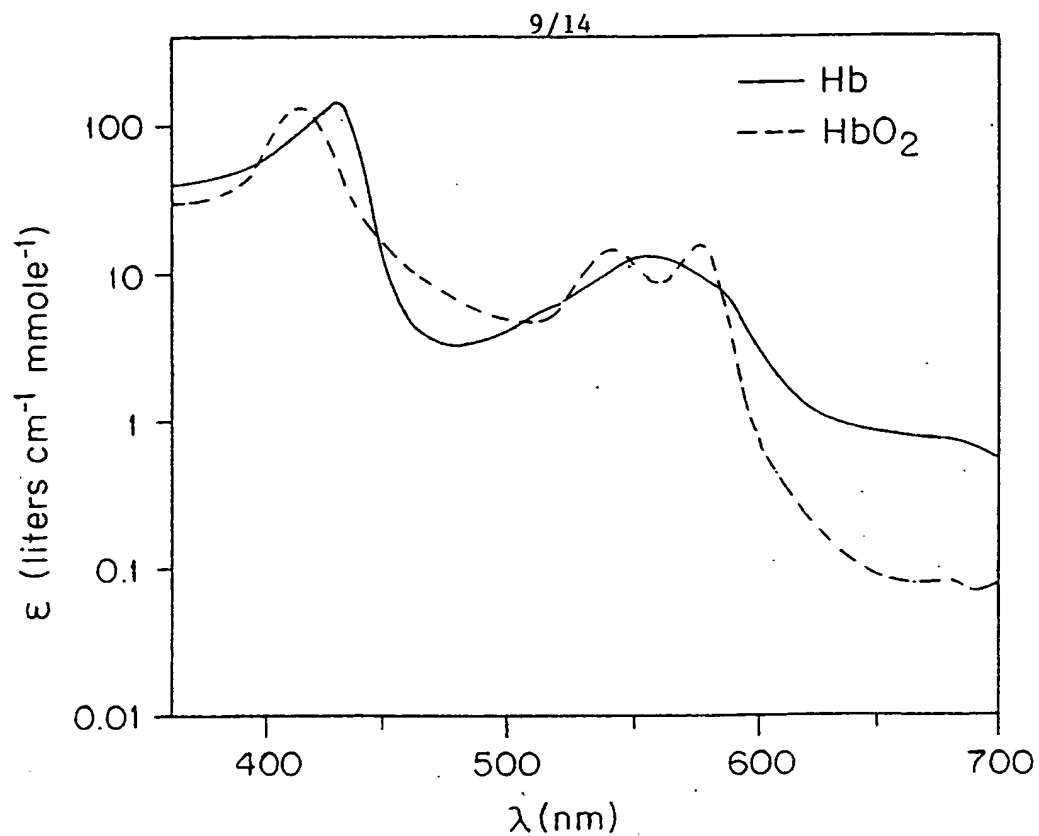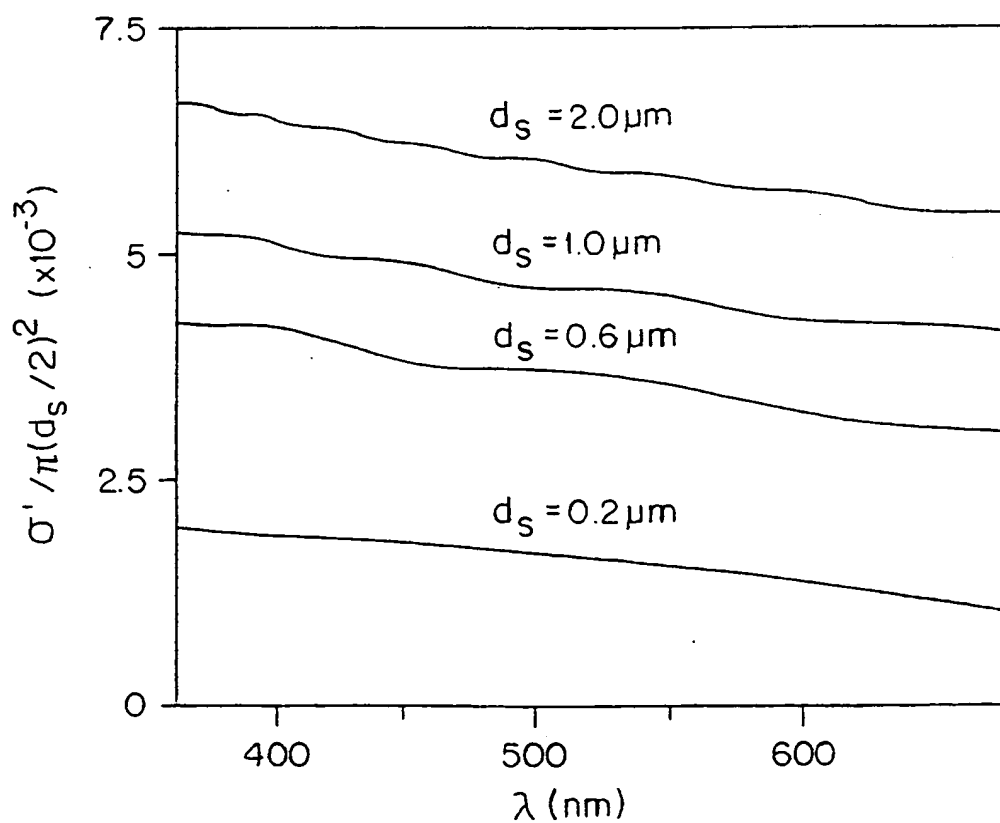
FIG. 8

FIG. 9

FIG. 10

This Page Blank (uspto)
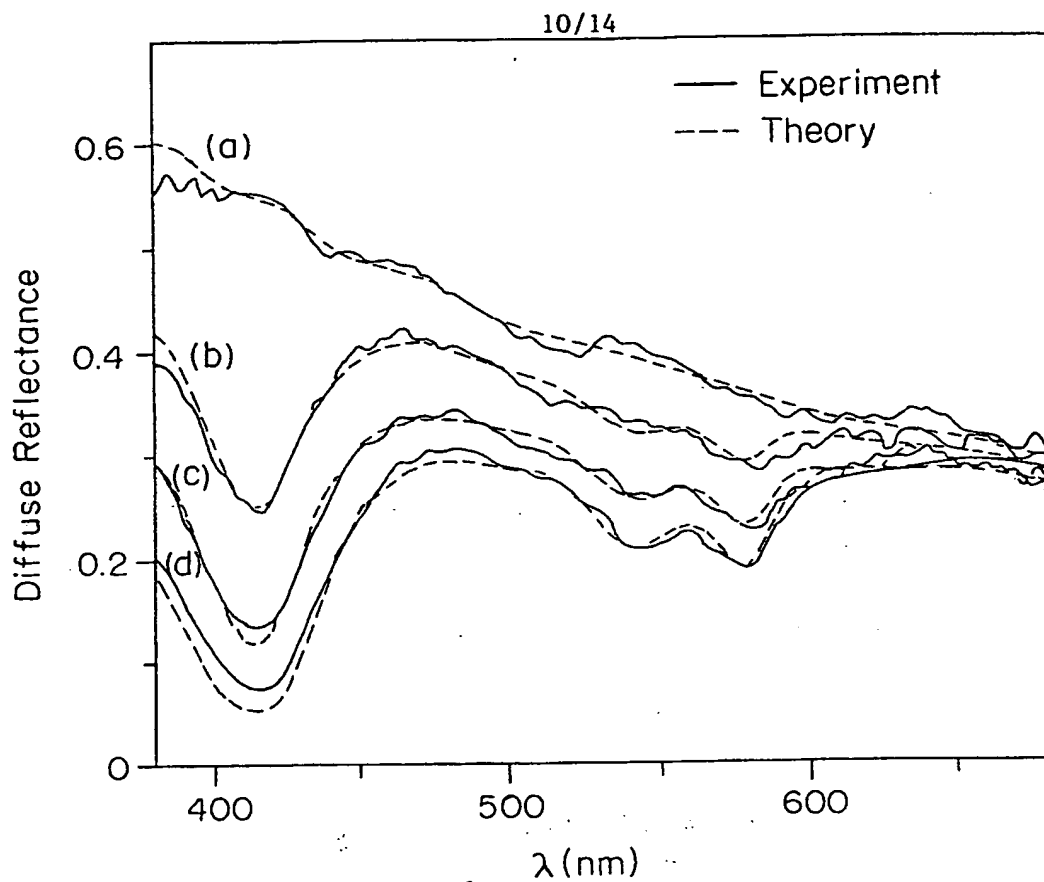
FIG. 11
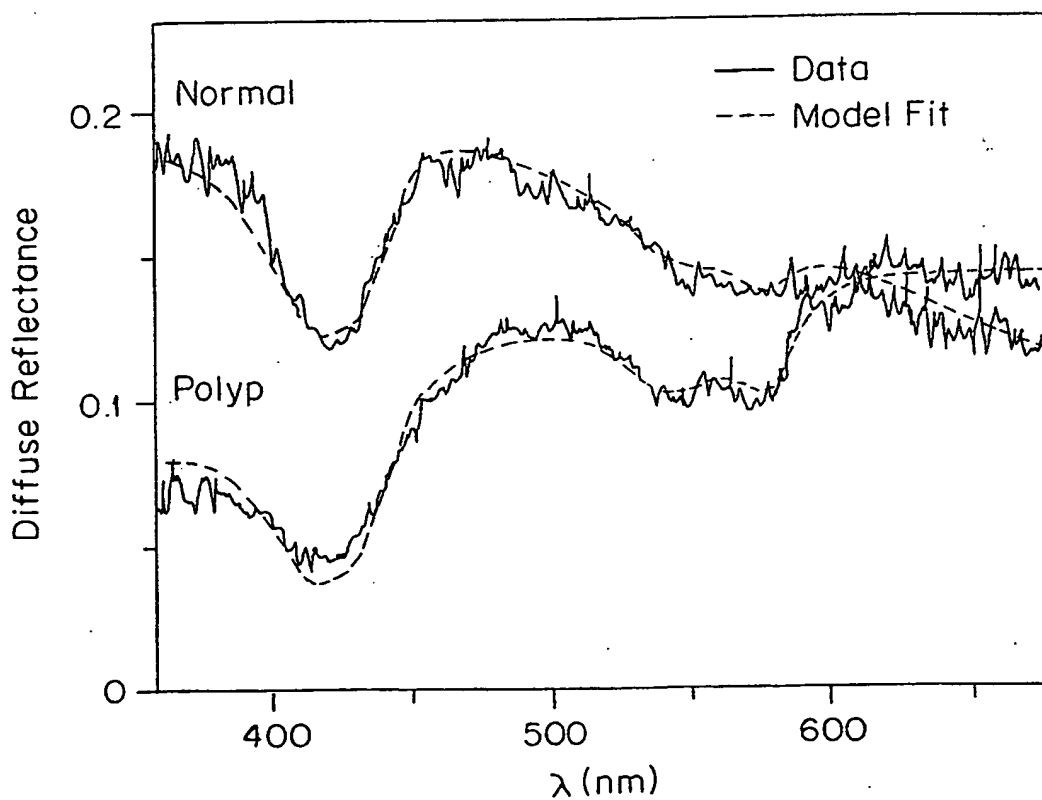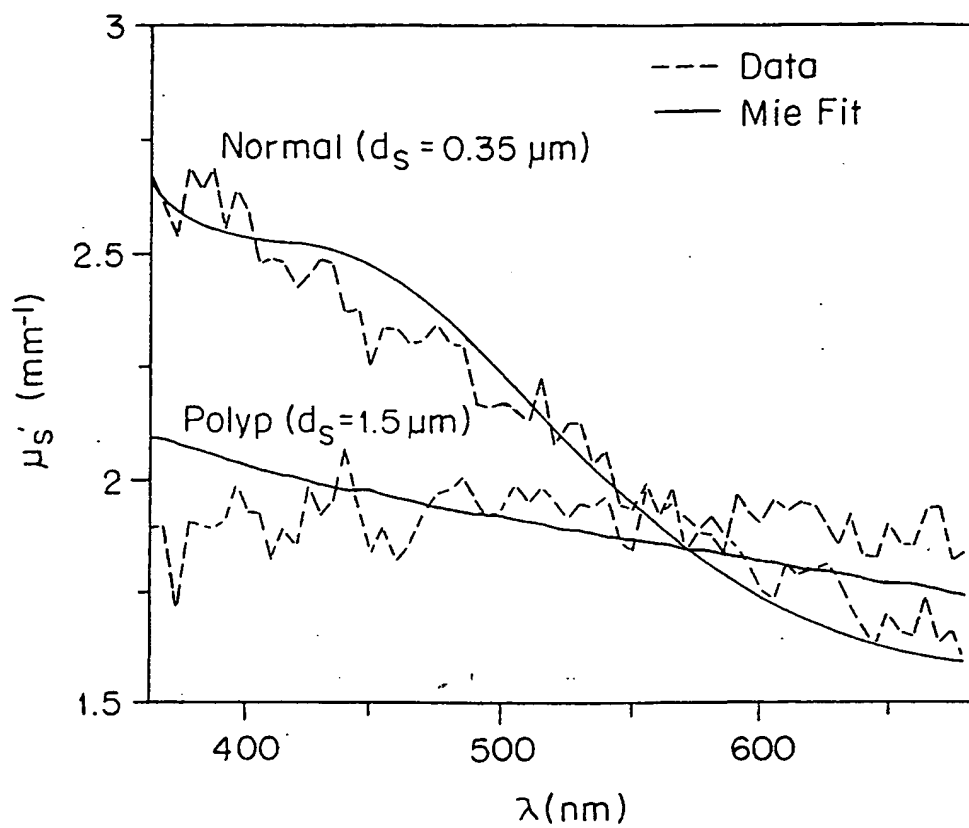

FIG 12
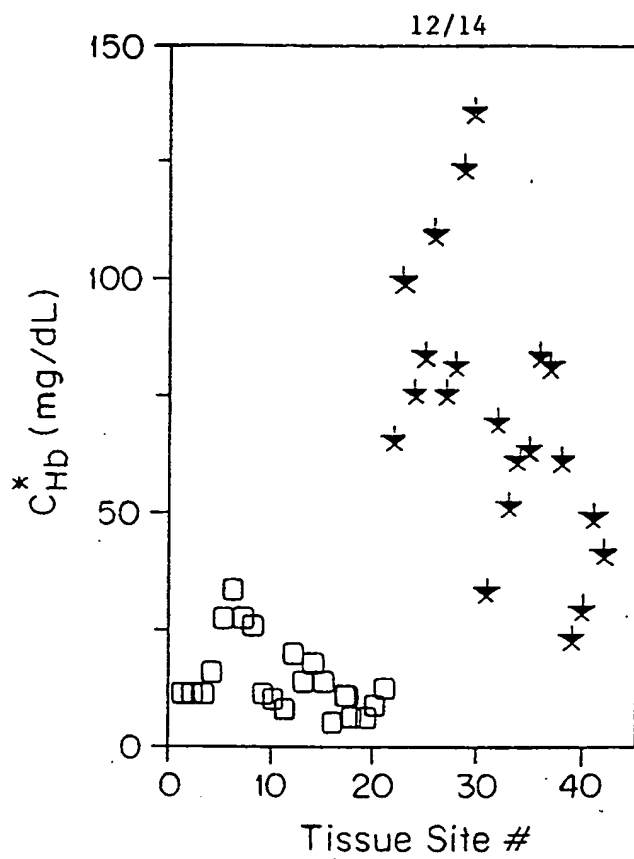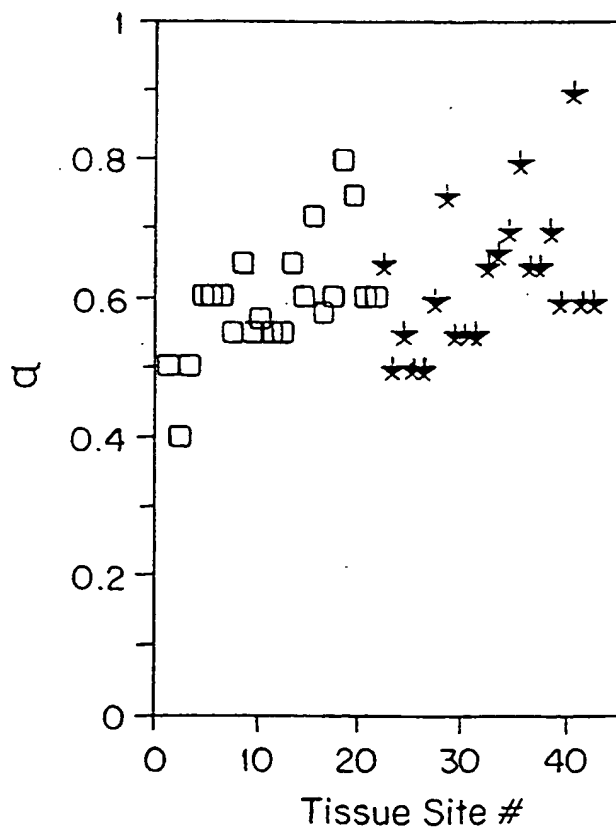
This Page Blank (uspto)

FIG. 13
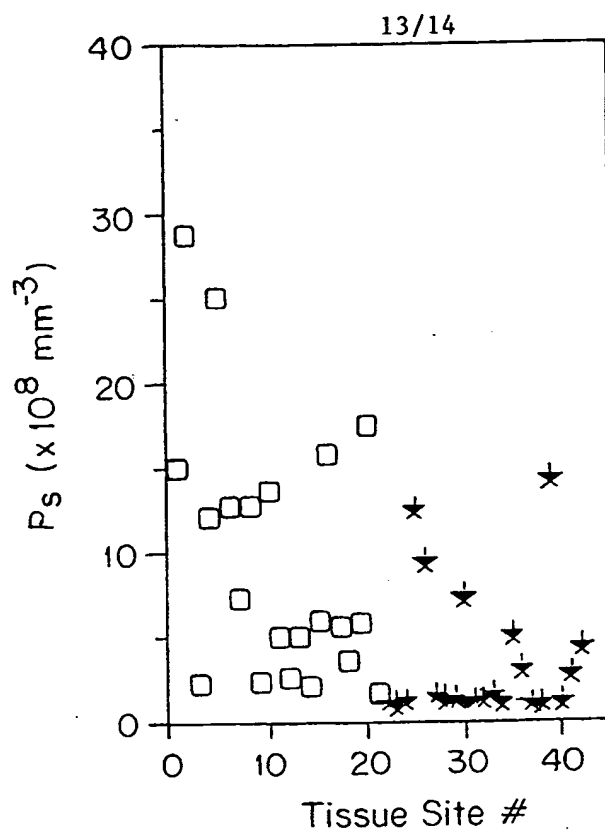
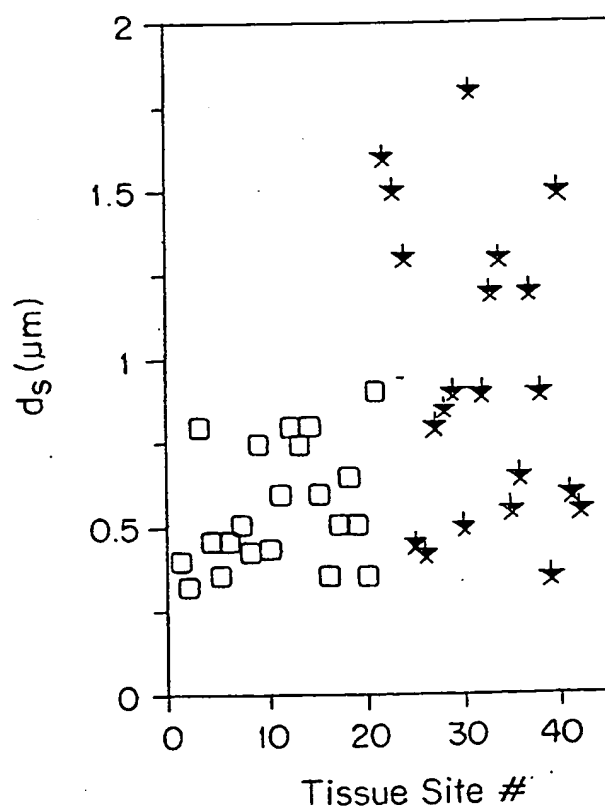This Page Blank (uspto)

FIG. 14A

This Page Blank (uspto)
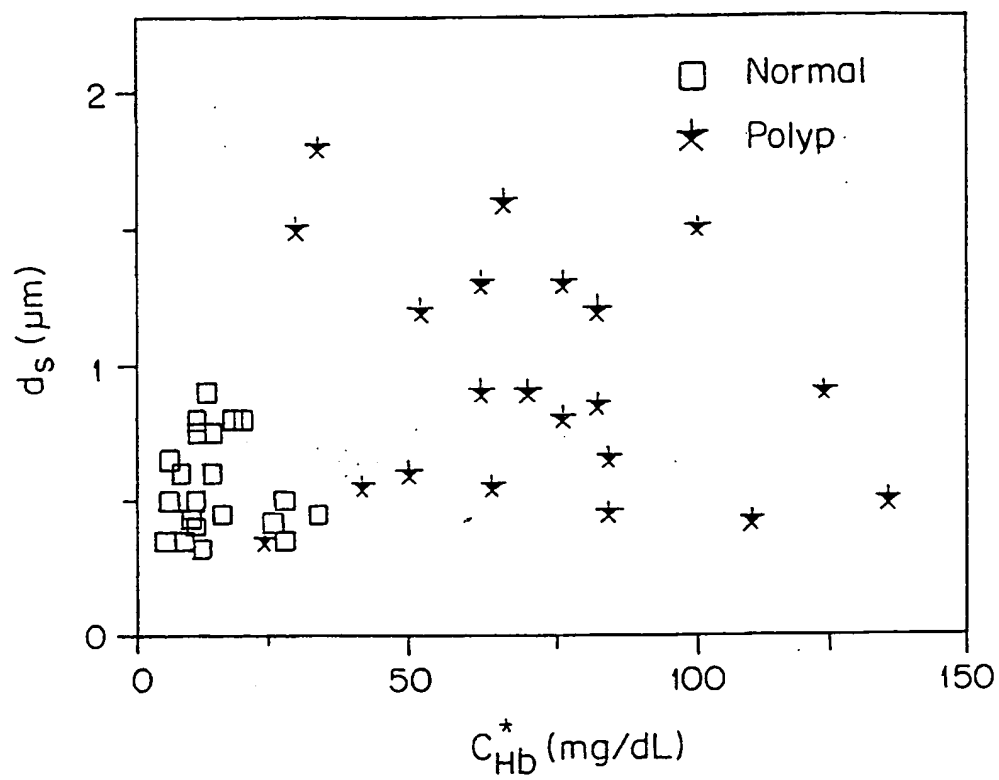
FIG. I4C

FIG. I4D

This Page Blank (uspto)

FIG. 15

This Page Blank (uspto)

INTERNATIONAL SEARCH REPORT

A. CLASSIFICATION OF SUBJECT MATTER
IPC 6   A61B5/00

According to International Patent Classification (IPC) or to both national classification and IPC

B. FIELDS SEARCHED

Minimum documentation searched (classification system followed by classification symbols)
IPC 6   A61B

Documentation searched other than minimum documentation to the extent that such documents are included in the fields searched

Electronic data base consulted during the international search (name of data base and, where practical, search terms used)

C. DOCUMENTS CONSIDERED TO BE RELEVANT

Category °	Citation of document, with indication, where appropriate, of the relevant passages	Relevant to claim No.
X	US 4 718 417 A (C. KITTRELL ET AL.) 12 January 1988	1-4,7
X	see column 19, line 26 - column 20, line 11	9-12,15, 17,18,20
X	see column 24, line 4 - line 66	23,25,26
X	see figures 21-24	30,32-34

X	US 4 281 931 A (T. CHIKAMA) 4 August 1981	1-6
X	see column 1, line 9-15	9-14,17
X	see column 1, line 64 - column 2, line 7	18,20-22
X	see column 4, line 32 - column 5, line 17	24,30, 32-34
A		25,26,28

	-/--	

| X | Further documents are listed in the continuation of box C. | X | Patent family members are listed in annex. |

° Special categories of cited documents :

"A" document defining the general state of the art which is not considered to be of particular relevance

"E" earlier document but published on or after the international filing date

"L" document which may throw doubts on priority claim(s) or which is cited to establish the publication date of another citation or other special reason (as specified)

"O" document referring to an oral disclosure, use, exhibition or other means

"P" document published prior to the international filing date but later than the priority date claimed

"T" later document published after the international filing date or priority date and not in conflict with the application but cited to understand the principle or theory underlying the invention

"X" document of particular relevance; the claimed invention cannot be considered novel or cannot be considered to involve an inventive step when the document is taken alone

"Y" document of particular relevance; the claimed invention cannot be considered to involve an inventive step when the document is combined with one or more other such documents, such combination being obvious to a person skilled in the art.

"&" document member of the same patent family

Date of the actual completion of the international search	Date of mailing of the international search report
26 January 1999	01/02/1999

Name and mailing address of the ISA	Authorized officer
European Patent Office, P.B. 5818 Patentlaan 2 NL - 2280 HV Rijswijk Tel. (+31-70) 340-2040, Tx. 31 651 epo nl, Fax (+31-70) 340-3016	Rieb. K.D.

INTERNATIONAL SEARCH REPORT

C.(Continuation) DOCUMENTS CONSIDERED TO BE RELEVANT

Category °	Citation of document, with indication,where appropriate, of the relevant passages	Relevant to claim No.
X	WO 92 14399 A (MIT) 3 September 1992	1-4,7
X	see page 2, line 4 - line 29	9-12,15
X	see page 8, line 16 - page 9, line 13	17-20,25
X	see page 18, line 23 - page 19, line 24	26,30-34
X	& US 5 280 788 A	
	cited in the application	

INTERNATIONAL SEARCH REPORT

Information on patent family members

Patent document cited in search report		Publication date	Patent family member(s)		Publication date
US 4718417	A	12-01-1988	CA	1279901 A	05-02-1991 −
			CA	1339056 A	29-07-1997
			CA	1317641 A	11-05-1993
			CA	1329655 A	17-05-1994
			DK	130586 A	23-09-1986
			FI	861209 A	23-09-1986
			JP	2589674 B	12-03-1997
			JP	61257638 A	15-11-1986
			JP	2739933 B	15-04-1998
			JP	9117407 A	06-05-1997
US 4281931	A	04-08-1981	NONE		
WO 9214399	A	03-09-1992	US	5280788 A	25-01-1994
			EP	0575472 A	29-12-1993

This Page Blank (uspto)